UNIVERSITÄTSKLINIKUM HAMBURG-EPPENDORF

Zentrum für experimentelle Medizin
Institut für Neuroanatomie

Institutsdirektorin: Frau Prof. Dr. med. Gabriele Rune

Functions of GPER1 in the temporoammonic pathway

Dissertation

zur Erlangung des Grades eines Doktors der Medizin
an der Medizinischen Fakultät der Universität Hamburg.

vorgelegt von:

Xiaoyu Li
aus Jiangsu (China)

Hamburg 2020

Angenommen von der
Medizinischen Fakultät der Universität Hamburg am: 27.02.2020

Veröffentlicht mit Genehmigung der
Medizinischen Fakultät der Universität Hamburg.

Prüfungsausschuss, der/die Vorsitzende: Prof. Dr. med. Gabriele M. Rune

Prüfungsausschuss, zweite/r Gutachter/in: Prof. Dr. Markus Glatzel

Contents

1. Introduction

1.1 Hippocampus

The hippocampus, which is located beneath the medial temporal lobe, is a part of the limbic system in the brain. It plays important roles in memory formation and spatial navigation. Anatomically, hippocampus belongs to the archicortex, which is histologically characterized by only three layers (Waxman, 2013). Although there is no consensus for the term hippocampal formation, which is used to describe the hippocampus proper and its related regions, it consists of three parts in general: hippocampus proper (also called *cornu ammonis*, CA), dentate gyrus (DG) and subiculum (Martin, 2003). The hippocampus proper is divided into 3 subfields: CA1, CA2 and CA3, which are subdivided into layers: stratum oriens (SO), stratum pyramidal (SP), stratum radiatum (SR), stratum lacunocum-moleculare (SLM) and stratum lucidum (SL). SL is only present in CA3 and refers specifically to the area, in which mossy fibers terminate (Standring, 2015; Figure 1.1). The dentate gyrus has a prominent trilaminar structure: the overlying molecular layer, the dense granule cell layer in between and the underlying polymorphic layer, which is also called the hilus of the dentate gyrus. The entorhinal inputs are precisely transferred into the outer two-thirds of the molecular layer (Amaral et al., 2007).

The hippocampus receives its main input via the entorhinal cortex (EC). Generally, there are two efferent synaptic pathways that transfer excitatory inputs from EC into CA1 hippocampus (Maccaferri, 2011). The first is the traditional perforant path (PP), which originates from layer II stellate cells in EC (Witter et al., 2017). The PP axons from the medial and lateral EC innervate the middle and outer third of granule cell dendrites in DG, respectively. Then, the granule cells in DG project to CA3 pyramidal cell dendrites in SL via the mossy fibers. CA3 pyramidal cell axons branch in CA3. One branch leaves the hippocampus via the fornix while the other branch forms synapses with the proximal dendrites of pyramidal cells in CA1 SR through the Schaffer collaterals. Taken together, this

indirect way of excitatory synaptic transmission from EC to CA1 is termed the "trisynaptic path" (Yeckel and Berger, 1990).

In addition to the "trisynaptic path", there is also a direct excitatory synaptic connection between EC and CA1, termed the "temporoammonic path (TA)". It originates from EC neurons in layer III and terminates in SLM, where the distal dendrites of CA1 pyramidal cells are located (Neves et al., 2008; Maccaferri, 2011; Figure 1.1).
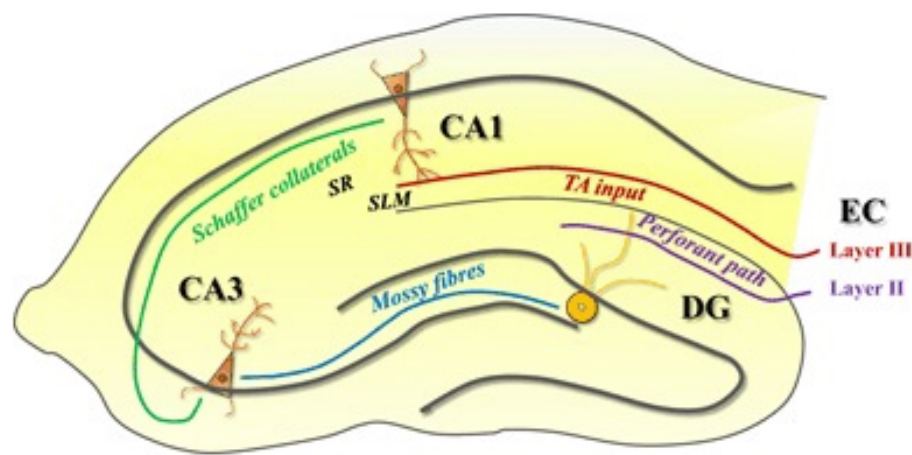
Figure 1.1 Anatomy and circuits of the hippocampus (from McGregor and Harvey, 2019)

Hippocampus is a highly plastic brain structure and is considered to be crucial for learning and memory. Large amounts of research have been performed to explore the synaptic transmission of indirect PP and ample evidence has confirmed its important role in memory formation and navigation. In contrast, comparably few studies have focused yet on understanding the roles of the direct TA. These studies indicate that the TA could be specifically important for the formation and consolidation of long-term memory (Brun et al., 2002; Remondes and Schuman, 2004; Li et al., 2017), and could be involved in the generation of temporal association memory (Suh et al., 2011).

Comparing the direct and indirect pathways, Manns et al. (2007) further suggested that the synaptic transmission from EC to CA1 via the TA is involved in memory encoding, while input from CA3 to CA1 via Schaffer collaterals appears to be more important for memory retrieval. However, it is generally little understood how the TA processes the information

from EC to hippocampus, and which regulatory mechanisms influence its synaptic transmission. Work from our laboratory recently suggested regulatory functions of estrogens at TA synapses (Meseke et al., 2018). In my thesis, I extended these studies, thereby focusing on the roles of the *G*-Protein-coupled *E*strogen *R*eceptor 1 (GPER1, previously termed GPR30, Carmeci et al., 1997).

1.2 Estrogens

Estrogens comprise a group of sexual steroid hormones, which are generated from cholesterol by a series of catalytic reactions (Fester et al., 2009, Figure 1.2). Of the three major compounds - estrone (E1), estradiol (E2) and estriol (E3), E2 (precisely: 17β-estradiol) is the most potent and the most important for non-pregnant women during reproductive years. However, estrogens are not only produced in female reproductive organs, but can be generated in many other tissues, including the brain (see below). Moreover, the functions of estrogens are not limited to the regulation of female reproduction, but have, for instance, also long been known to work as "neuromodulators" in the brain (Prange-Kiel et al., 2003; Woolley, 2007; Hojo et al., 2008; Fester and Rune, 2015).

In the early 1990s, the group of McEwen at Rockefeller University observed that removal of the ovaries in adult female rats resulted in a decrease of apical dendritic spine density in hippocampal CA1, which was rescued by E2 replacement (Gould et al., 1990). Furthermore, the group found that the density of both dendritic spine and spine synapses in SR region of CA1 fluctuated during the estrous cycle, with low concentrations of estradiol resulting in a lower density and high concentrations resulting in a higher density of both spines and synapses (Gould et al., 1990; Woolley and McEwen, 1992).

While these findings suggested that peripheral estradiol, secreted into the blood circulation and arriving at the target region in brain via the blood-brain-barrier (Paul and Purdy, 1992), can act as a neuroactive steroid, other groups showed that the final enzyme converting testosterone to E2, aromatase (AROM), is expressed in the brain and that neurons can

generate E2 themselves (Prange-Kiel et al., 2003; Hojo et al., 2004; Kretz et al., 2004). Thus, besides being a neuroactive hormone, E2 can also act as a "neurosteroid", that is locally synthesized in the brain and does not require steroidogenic glands (Baulieu and Robel, 1990; Balthazart and Ball, 2006).
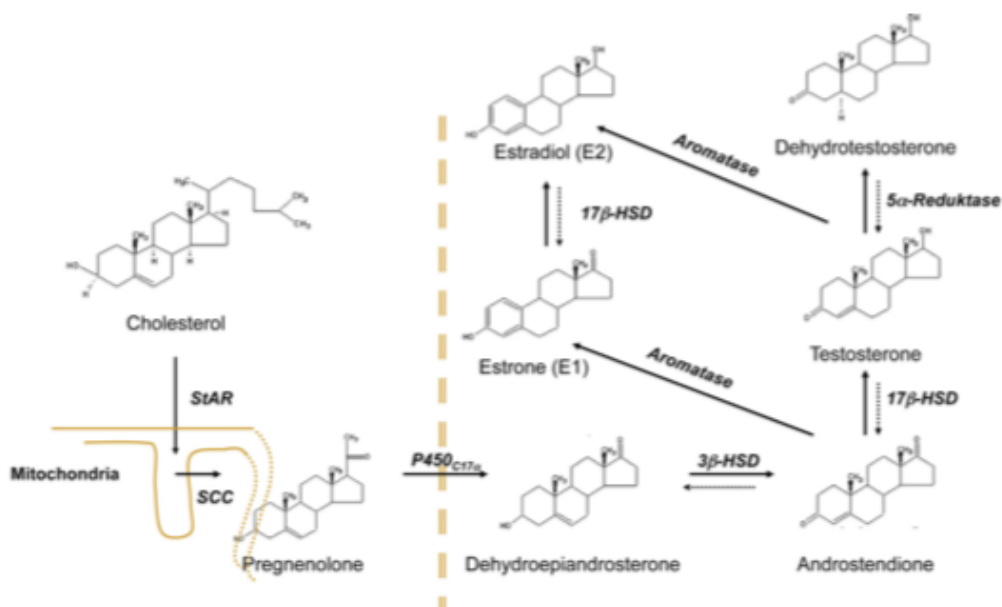
Figure 1.2 Biosynthesis of 17β-estradiol (from Prange-Kiel et al., 2013)

Since it has been recognized that E2 acts as a neuromodulator in the brain, several functions have been discovered. Thus, it was shown to modulate several parameters of synaptic plasticity, such as spine synapse density (Kretz et al., 2004; Bender et al., 2010, 2017; Zhou et al., 2010; Vierk et al., 2012), spinogenesis (Mukai et al., 2007; Srivastava et al., 2008; Hasegawa et al., 2015), synaptic protein expression (Kretz et al., 2004; Jelks et al., 2007; Fester et al., 2017), and the modulation of long-term potentiation (LTP) and long-term depression (LTD) (Foy et al., 1999; Kramar et al., 2009; Vierk et al., 2012; Bender et al., 2017). Importantly, E2 appears to have beneficial effects even in the human brain, e.g., by enhancing learning and memory functions (Hojo et al., 2008; Bayer et al., 2015) or providing neuroprotection in global cerebral ischemia (Tang et al., 2014) and Alzheimer Disease (AD) (Janicki and Schupf, 2010; Prange-Kiel et al., 2016). Additionally, it can affect

dopamine-dependent cognitive diseases, such as Parkinson's Disease, schizophrenia, and addiction (Almey et al., 2015).

1.3 Estrogen receptors

Estradiol requires the involvement of estrogen receptors (ERs) to exert its effects. Generally, there are two ways considered for estradiol signaling (Figure 1.3). One is the classical way, also known as the genomic way/slow way. It takes hours to days to manifest, and functions via gene transcription. Briefly, estradiol passes through cell membrane because of its hydrophobic steroid structure and then binds in the cytosol to the classical estrogen receptors (ERα, ERβ; see below) to form the E2-ER complex. This complex translocates into the nucleus and stimulates gene transcription with the help of co-regulators (McEwen and Alves, 1999; Srivastava et al., 2011; Frick et al., 2015). The alternative, non-classical way, also called non-genomical way/ fast way, generates effects via the activation of cell signaling cascades and/or epigenetic alterations (Vasudevan and Pfaff, 2008; Frick et al., 2015). The non-classical way may in some respect also involve the classical, mainly cytosol-based receptors ERα and ERβ (see Figure 1.3). But recently, a membrane-bound G-protein-coupled estrogen receptor (GPER1) has been discovered, which is optimally suited to mediate the fast effects of estradiol binding.
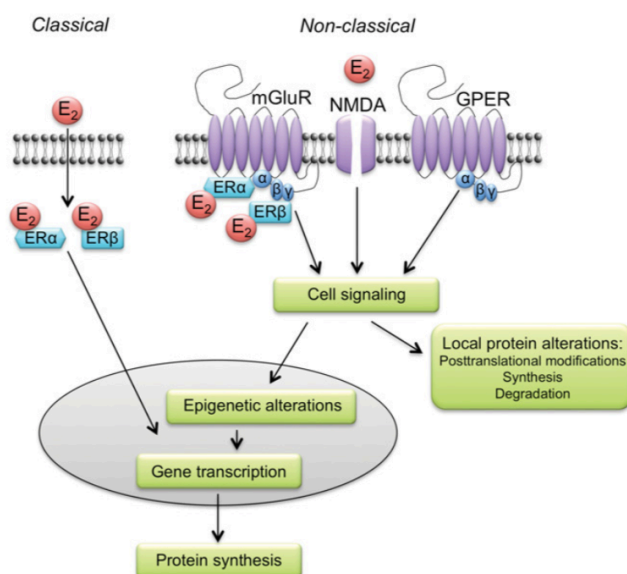
Figure 1.3 Genomic and non-genomic mechanism of E2 action (from Frick et al., 2015)

1.4 GPER1

GPER1, previously termed GPR30, was first discovered in a breast carcinoma cell line (MCF7) using differential cDNA library screening techniques in 1997 (Carmeci et al., 1997). It belongs to the "seven-transmembrane G-protein-coupled receptor (GPCR)" family and was initially identified as an orphan receptor. In 2005, Thomas et al. (2005) found that GPR30 could be activated by estradiol *in vitro*. Revankar et al. (2005) found it localizing to the endoplasmic reticulum and showing specific binding activity to E2. These two published studies established GPR30 as a membrane-bound ER, which was renamed GPER1 in 2007 (for review, see Prossnitz and Barton, 2011). Subsequent studies showed that GPER1 is also expressed on the plasma membrane of neurons in the hypothalamus and hippocampus, indicating that GPER1 activation could have effects on neural transmission in these brain regions (Funakoshi et al., 2006; Prossnitz et al., 2008; Akama et al., 2013; Srivastava and Evans, 2013; Almey et al., 2015; Waters et al., 2015). In hippocampal CA1, Akama et al. (2013) reported GPER1 localizing to dendritic spines of pyramidal cells in mice by electron microscopy, which was later confirmed by Waters et al. (2015). In CA1 dendritic spines, GPER1 is frequently found at the postsynaptic density, where it is associated with the scaffolding protein PSD95 (Akama et al., 2013; Waters et al., 2015), suggesting a mainly postsynaptic function of the receptor. However, evidence exists suggesting that GPER1 may also function presynaptically, e.g., in dorsal striatum (Almey et al., 2012) and hippocampus (Waters et al., 2015).

1.5 GPER1 and neural plasticity

GPER1 is thought to be involved in the non-genomic pathway of estradiol signaling and thus may have effects on the estrogen-modulated neuroplasticity and neuroprotection in the brain. Indeed, several studies have shown that GPER1 activation affects learning and memory processes, taking advantage of the availability of highly selective receptor agonists (G1, Bologa et al., 2006) and antagonist (G15, G36; Dennis et al., 2009, 2011). Thus, improved spatial recognition learning was observed in ovariectomized rats after treatment

with G1 for 24 and 48 hours, replicating the effects that are seen after low-dose treatment with estradiol (Hawley et al., 2014). It further has been reported that G1 enhances, while G15 impairs, spatial learning in ovariectomized rats by the method of a delayed-matching-to-position (DMP) T-maze task (Hammond et al., 2009, 2012). Additionally, increased dendritic spine density was observed within 40 min in SR region of CA1 after subcutaneously administration with G1 in ovariectomized CD1 mice (Gabor et al., 2015). GPER1 could also take effect on neuroprotection. Thus, Tang et al. (2014) reported that G1 exerts neuroprotection against global cerebral ischemia by activating Akt and ERK (the pro-survival kinases) rapidly. In a Parkinson's disease mouse model, G1 was identified to attenuate the decrease of dopamine in myenteric neurons and enteric macrophage infiltration while G15 could block such anti-inflammatory and neuroprotective effects of G1 (Côté et al., 2015).

1.6 Aims of the study

From the findings presented above, it is apparent that GPER1 needs to be considered an important mediator of E2-induced neuronal plasticity in hippocampus. However, studies on its roles have so far focused on the SR region in CA1, the termination zone of the Schaffer collaterals, but have ignored SLM, the termination zone of the TA, which is also target of estradiol-mediated neuroplasticity, as Smith et al. (2016) have found an altered dendritic spine density in SLM after E2-injection for 24 hours in female rats. Moreover, our group found recently that the enrichment of the hyperpolarization-activated ion channel HCN1, which regulates membrane properties (Bender and Baram, 2008), in the distal dendrites of CA1 pyramidal cells is regulated by E2, as application E2 to organotypic hippocampal slice cultures enhanced the expression of HCN1 in CA1 SLM (Meseke et al., 2018). This effect was replicated by application of the GPER1-agonist G1 and was prevented if E2 was applied together with the GPER1-antagonist G36, thus strongly suggesting that it is mediated by GPER1 (Meseke et al., 2018). GPER1, in turn, is prominently expressed in

SLM and thus optimally localized to mediate E2-effects on neuroplasticity of the TA (Waters et al., 2015; Meseke et al., 2018).

In my thesis, I used a mouse model that allows identification of individual neurons in CA1 (Thy1-GFP transgenic mice, Feng et al., 2000a) to explore the functions of GPER1 specifically at temporoammonic-CA1 synapses in SLM. The following questions will be addressed:

1) Does GPER1 signaling affect spine density in SLM?

2) Does GPER1 signaling affect spine synapse formation in SLM?

3) Dose GPER1 signaling affect the hippocampal expression of pre/post synaptic proteins?

To address these questions, the following experiments were performed: Firstly, I used western blot and immunohistochemistry to demonstrate the expression of GPER1 in hippocampus and EC in mice. Secondly, I used organotypic entorhinal-hippocampal slice cultures generated from early postnatal Thy1-GFP-mice to determine effects of G1 and E2 on SLM spine density by confocal microscopy. Thirdly, I used organotypic-entorhino-hippocampal slices generated from wild type mice to determine effects of G1 on SLM spine synapse density by electron microscopy. Fourthly, organotypic cultures from wild-type mice were used to determine effects of G1- and E2-treatment on the expression of pre- or postsynaptic proteins in the culture tissue, in general. Importantly, care was taken to analyze male and female tissue separately, in order to identify potential sex differences.

2. Material and Methods

2.1 Experimental animals

C57BL / 6J wild type (WT) and Thy1-eGFP mice were used for this project. All mice were housed in the animal facility of the University Medical Center Hamburg-Eppendorf. The animals were kept in a constant day-night cycle, with access to food and water ad libitum. All experiments were performed in accordance with institutional guidelines for animal welfare. Animals were used at different ages for experiments, including early postnatal (postnatal day [P] 3-10), adolescent (P11-20) and adult stages (8-9 weeks old) for developmental time course analysis (P3, P10, P17), organotypic slice cultures (P7-8), and immunohistochemistry and Western Blot analysis of GPER1 expression (P13 and adult).

2.2 Materials

2.2.1 Instruments and Equipment

Analysis scale	SARTORIUS
Bio-Photometer	EPPENDORF
Boxes for slides	VWR
Centrifuge	HETTICH
Centrifuge 5417R	EPPENDORF
Chemiluminescence camera	FUSION SL2. VILBER
CO2-Incubator, 37°C	HERAEUS
Cover slips, 24*46mm, 24*60mm	MARIENFELD
Cutfix Surgical Disposable Scalpel	BRAUN
Diamant Knife	DIATOM
Desinfectant	BODE
Dissection tools	F.S.T
Document foils	LEITZ
Electrophoresis constant power supply ECPS 3000/150	PHARMACIE
Electrophoresis constant power supply EPS 3501 XL	AMERSHAM PHARMACIE BIOTECH

Eletron microscope	CM 100, PHILIP, PW 602
Embedding forms	PLANO
Ep T.I.P.S. Standard, different sizes	EPPENDORG AG
Falcon Multiwell Cell Culture Plate	BECTON DICKINSON LAB
Falcon tubes, 15 mL, 50 mL	GREINER BIO-ONE
Filter paper	SCHLEICHER-SCHÜLL
Forceps	MERCK
Freezer (-25°C, -80°C)	LIEBHERR
Fridge (4°C)	BOSCH/LIEBHERR
Gelatine capsule	PLANO
Gel-Combs	BIO-RAD
Glass slide	ASSISTANT
Gloves, different sizes	KIMBERLY-CLARK
Heidemann spatula	AESCULAP DE
Incubator	MEMMERT
Laser Scanning Microscope	AXIOVERT 100 M ZEISS
Light-optical microscope	AXIONVERT 25 ZEISS
Microtome Blade S35	FEATHER
Microtome	REICHERT-JUNG
MiliCell® membranes	MILLIPORE
Nitrocellulose Blotting Membrane	SIGMA-ALDRICH
Pipettes, 100 mL and 2500 mL	EPPENDORF AG
Pipettes 2, 20,100 and 1000 µL	GILSON
One-time Cuvettes	ROTH
Parafilm	PECHINEY PLASTIC PACKAGING
Pasteur pipette	ASSISTANT
Photographic paper	TETENAL
Pipette tips for Pipetus 5, 10 und 25 mL	BECTON DICKINSON LAB
Pipette tips	EPPENDORF AG
Pipetus Akku	HIRSCHMANN
Scissors	FINE SCIENCE TOOLS
Tissue Chopper	H. SAUER
Ultramicrotome	REICHERT-JUNG
Tubes, 1, 2 and 5 mL	EPPENDORF AG
Wet Chamber	SELF-MADE, UKE

2.2.2 Chemicals

Ammonium persulfate (APS)	SIGMA
Aqua ad iniectabilia	BAXTER
Bio Rad Protein Assay	BIO-RAD LAB. GMBH
Bromophenol blue (BPB)	SIGMA
Bovine serum albumin (BSA)	MERCK
Carbonic acid	SOL SPA
ECL (Pierce® Western Blotting Substrate)	THERMO SCIENTIFIC
DAB Peroxidase (HRP) Substrate Kit	VECTOR LABORATORIES
4,6-diamidno-2-phenylindole (DAPI)	SIGMA
Delimiting pen	DAKO
Disodium phosphate (Na_2HPO_4)	MERCK
Dithiothreitol (DTT), 0.1 M	INVITROGEN
Dry ice	TMG
Entellan	MERCK
Ethanol, 100%	MERCK
Ethanol, 70%, 96%	Chemistry, UKE
Ethidium bromide	SERVA
Ethylendiaminetraacetat (EDTA)	MERCK
Fluorescent Mounting Medium	DAKO
Glucose, 50%	FRESENIUS KABI
Glutaraldehyde, 25%	MERCK
Glutaraldehyde solution, 25%	MERCK
Glycerin	SIGMA
Glycin	ROTH
HM 560 (cryostat)	MICROM
Hydrochloric acid (HCl)	MERCK
Immobilon™ Western chemiluminescent HRP substrate	MERCK MILLIPORE
Lead citrate	MERCK
L-Glutamine, 200 nM	SIGMA
Methanol	J.T. BAKER
2-methylbutan	MERCK
Milk powder (non-fat)	HEIRLER
Monosodium phosphate (NaH_2PO_4)	MERCK
Natriumphosphate buffer	MERCK
Neurobasal™ – A Medium, minus Phenol Red	Thermo Fisher

Nitrogen	Chemistry, UKE
Normal Goat Serum (NGS)	SIGMA
NP40 Alternative	CALBIOCHEM
Osmiumtetroxide (OsO$_4$)	ROTH
Oxygen	SOL SPA
Penicillin-Streptomycin	INVITROGEN
Paraformaldehyd (PFA)	MERCK
PageRuler™ Prestained Protein Ladder	Thermo Fisher
Phosphate Buffered saline (PBS)-Tablets	GIBCO
PhosStop™ phosphatase inhibitor tablets	ROCHE
Ponceau-Rot,	MERCK
cOmplete Protease Inhibitor EDTA-Free	ROCHE
Rotiphorese-Gel 30% (Acrylamid)	ROTH
Sodium dodecylsulfate (SDS)	FLUKA
Sodium bicarbonate (NaHCO$_3$) solution, 7.5%	MERCK
Sodium deoxycholate	SIGMA
Sodium hydroxide (NaOH)	MERCK
Sucrose	MERCK
Tissue Tek® O.C.T.™ Compound	SAKURA
Tris	ROTH
Triton-X	SIGMA
Tween	SIGMA
VECTASTAIN® Elite® ABC HRP Kit	VECTOR LABORATORIES

2.2.3 Solutions

2.2.3.1 Buffers

Phosphate buffered saline (1x PBS)

- 1 tablet of PBS

- add 500 mL distilled water

- adjust pH to 7.4 with NaOH (1 mol/L) or HCl (1 mol/L)

Phosphate Buffer (PB), 0.1 M

- 77 mL Na$_2$HPO$_4$, 0.5 M

- 23 mL NaH$_2$PO$_4$, 0.5 M

- add distilled water to the final volume of 500 mL

Phosphate Buffer (PB), 0.2 M

- 5.52 g NaH_2PO_4

- 42.88 g Na_2HPO_4

- add distilled water to the final volume of 1000 mL

Sucrose buffer solution

- 6.846 g sucrose dissolved in 100 mL 0.2 M PB

2.2.3.2 Fixation solutions

Paraformaldehyde (PFA), 4%

- 40 g PFA dissolved in 1000mL PBS

- adjust pH to 7.4 with NaOH (1 mol/L) or HCl (1 mol/L)

Glutaradehyde, 2.5%, in 0.1 M PB

- 50 mL glutaradehyde, 25%

- 77 mL Na_2HPO_4, 0.5 M

- 23 mL NaH_2PO_4, 0.5 M

- add distilled water to the final volume of 500 mL

- adjust pH to 7.4 with NaOH (1 mol/L) or HCl (1 mol/L)

Osmiumtetroxide (OsO_4) solution, 2%

- 2 g OsO_4 dissolved in 100 mL distilled water

2.2.3.3 Culture media

Preparation medium

- Neurobasal A

Incubation medium

- 45 mL Neurobasal A

- 5 mL Fetal bovine serum (FBS), 10%

- 500 µL B27

- 125 µL L-glutamine, 200 mM

- 500 µL Penicillin-Streptomycin (PS) solution,

- 500 µL 30% glucose in Neurobasal A

2.2.3.4 Western Blot

RIPA Buffer

- 1.5 mL NaCl, 150 mM

- 2.5 mL Tris, 50 mM, pH=7.5

- 5 mL NP40 Alternative, 1%

- 500 µL SDS, 0.1%

- 2.5 mL sodium deoxycholate, 0.5%

- 0.5 mL EDTA, 5 mM

- add cold ddH$_2$O to the final volume of 50 mL

- add a mixture of proteinase inhibitors before use: Protease inhibitor 1:25 (cOmplete), Phosphatase inhibitor 1:10 (PhosStop^{TM})

10% Sodium dodecyl sulfate (SDS)

- 50 g SDS

- add distilled water to the final volume of 500 mL

10% Ammonium persulfate (APS)

- 10 g APS

- add distilled water to the final volume of 100 mL

5x Laemmli sample buffer

- 1.54 g Dithiothreitol (DTT)

- 8 mL Tris/HCl, pH = 6.8

- 2 g SDS

- 10 mL glycerol

- dissolve the mixture above for 5 minutes at 65-80°C

- fill up with glycerol to the final volume of 20 mL

- approximately 4 mg bromophenol blue (BPB) was added as a tracking dye.

10x Laemmli running buffer

- 30 g Tris

- 144 g glycin

- 10 g SDS

- add distilled water to the final volume of 1000 mL

- dilute 1:10 with distilled water for 1x Laemmli running buffer working solution

10x Transfer buffer

- 29 g glycin

- 58 g Tris

- add distilled water to the final volume of 800 mL

1x Transfer buffer

- 80 mL 10x Transfer buffer

- 200 mL methanol

- add cold distilled water to the final volume of 1000 mL

10x PBS

- 87.66 g sodium chloride

- 2.7 g $NaH_2PO_4*H_2O$

- 14.31 g $Na_2HPO_4*2H_2O$

- add distilled water to the final volume of 1000 mL

- adjust pH to 7.4 with NaOH (1 mol/L) or HCl (1 mol/L)

PBS-Tween 20 0.3%

- 30 mL Tween 10%, 100 mL 10x PBS,

- add distilled water to the final volume of 1000 mL

Blocking solution

1) 5% milk solution

-5 g non-fat milk powder diluted in 100 mL 0.3% PBS-Tween

2) 5% BSA solution

- 5 g bovine serum albumin (BSA) diluted in 100 mL 0.3% PBS-Tween

2.2.4 Antibodies

Primary antibody	Source	Identifier	Type	Dilution
Rabbit anti-GPER1	Abcam	Cat#ab39742, RRID: AB_1141090	polyclonal	1:400 (IHC) 1:250 (WB)
Mouse anti-PSD95	sigma	Cat# P-246 RRID: AB_260911	monoclonal	1:250 (IHC) 1:2000 (WB)
Rabbit anti-GFP	Abcam	Cat#ab6556 RRID: AB_305564	polyclonal	1:2500 (IHC)
Rabbit anti-ITPKA	Proteintech	Cat#14270-1-AP RRID: AB_2129841	polyclonal	1:2000 (WB)
Rabbit anti-Spinophilin (Neurabin II)	Millipore	Cat#06-852 RRID: AB_310266	polyclonal	1:1000 (WB)

Rabbit anti-SNAP25	Abcam	Cat#ab41455 RRID: AB_945552	polyclonal	1:1000 (WB)
Rabbit anti-Cofilin	Cell Signaling	Cat#5175 RRID: AB_10622000	monoclonal	1:1000 (WB)
Rabbit anti-Phospho-Cofilin	Cell Signaling	Cat#3313 RRID: AB_2080597	monoclonal	1:300 (WB)
Mouse anti-GAPDH	Ambion	Cat#AM4300 RRID: AB_437392	monoclonal	1:10000 (WB)
Mouse anti-β-actin	Abcam	Cat#ab8224 RRID: AB_449644	monoclonal	1:1000 (WB)

Table 2.1: Primary antibodies used for IHC and WB

Secondary antibody	Source	Identifier	dilution
Biotinylated goat anti-Rabbit IgG	VECTOR LABORATORIES	Cat#BA-1000 RRID: AB_2313606	1:250 (IHC)
Goat-anti-Rabbit Alexa Fluor 488	Molecular Probes	Cat#A11008 RRID: AB_143165	1:500 (IHC)
Donkey-anti-Rabbit Alexa Fluor 647	Molecular Probes	Cat#A31573 RRID: AB_2536183	1:500 (IHC)
Goat-anti-Mouse-HRP	Jackson Immuno Research	Cat#115035174 RRID: AB_2338512	1:2500 (WB)
Donkey-anti-Rabbit-HRP	Jackson Immuno Research	Cat#211032171 RRID: AB_2339149	1:2500 (WB)

Table 2.2: Secondary antibodies used for IHC and WB

2.3 Methods

2.3.1 Tissue preparation

For immunohistochemistry (IHC), adult (8-9 weeks) and young postnatal mice (P12-13) were perfused with 4% PFA to preserve the cellular and sub-cellular structure of the brain tissue. Briefly, the mouse was placed in a small chamber, anesthetized first with a mixture of oxygen and carbon dioxide and then euthanized with pure carbon dioxide. The mouse was subsequently fixed with a tape on a metal table in a supine position. The xiphoid was exposed by a gentle cut through the skin using surgical scissors. Then, the abdominal muscles were cut to exposure the liver and the mouse ribs were cut along the midaxillary line of both sides to expose the heart. A small opening in the cardiac apex was cut with ophthalmic scissors, then the infusion needle was quickly inserted into the left ventricle and

the needle fixed with hemostatic forceps. The perfusion started after the right atrium was also opened. Firstly, 0.9% sodium chloride solution was perfused for 3-5 minutes to wash out the blood, recognizable by a paling of the liver. The perfusate was then replaced with 4% PFA fixation solution. Generally, when the fixation solution entered the mouse blood vessels, the limbs started twitching, indicating that the perfusate passed through the circulation system, including the brain. Fixation was then continued for 10-15 minutes and was regarded complete, when the liver had become hard. Subsequently, the mouse was decapitated, the skull was opened, and the mouse brain was carefully extracted using a Heidemann spatula. The brain was placed in a falcon tube containing 4% PFA for post-fixation for 24 hours.

After post-fixation, the brain was cryoprotected with 25% sucrose (in PBS) for 48 hours, deep frozen in 2-methylbutan (isopentan) on dry ice and stored at -80°C until further processing.

2.3.2 Organotypic slice culture

Organotypic entorhinol-hippocampal slice cultures, preserving the PP and the TA, were prepared from 7-8-day-old Thy1-eGFP or WT mice according to Stoppini et al. (1991). Briefly, pups were decapitated and the skullcap was cut along the median-sagittal line. The brain was removed and then placed on a small sponge soaked with sterile neurobasal A-medium. Brainstem and cerebellum were carefully removed and the brain was split into its two halves along the middle line. The hippocampus was now visible and could be gently separated, keeping the EC attached. Subsequently, hippocampus and EC were cut with a tissue chopper perpendicular to the longitudinal axis into 400 µm-thin slices, which were transferred to a petri dish filled with preparation medium. Under visual control (stereo microscope), slices were then gently separated from each other, but care was taken that adjacent slices ("sister cultures") stayed in pairs together. To control for eGFP-expression, one slice of a prospective thy1-eGFP mouse was observed under the fluorescence microscope. Slices were then transferred to MiliCell® membranes, but "sister cultures" were

always placed on two different membranes to serve as "experimental" and "control" slice, respectively. Membranes were placed in 6-well plates, each filled with 1 mL prewarmed and gassed (37°C, 5% CO_2) incubation medium. The slice cultures were maintained in a 37°C 95/5% CO_2 humidified incubator. Medium was changed every other day. After 4 days, the medium was supplemented for 24 hours or 48 hours either with G1 (20 nM) or E2 (2 nM) in the "experimental" group, or with the vehicle (DMSO) only in the "control" group.

At the end of treatment, slices from Thy1-eGFP positive pups, were fixed with 4% PFA for 2 hours at 4°C, then transferred to 25% sucrose (in PBS) for 4 hours at 4°C, and subsequently deep frozen with Tissue Tek® O.C.T.™ Compound on dry ice. It should be noted that this step was performed by another person to ensure that the following analyses were carried out "blinded". The frozen slice cultures were stored in the freezer at -20°C until further use for immunohistochemistry.

Similarly, organotypic entorhinal-hippocampal slice cultures, deriving from WT pups, were used for electron microscopy. For this purpose, slices were fixed with 2.5% glutaraldehyde for at least 48 hours and then further processed for EM as described below.

Another group of slices from WT pups was used for western blot analyses. These slices were carefully removed from the membrane and quickly frozen in liquid nitrogen after the treatment had ended.

2.3.3 Immunohistochemistry

Immunohistochemistry with mouse brain sections was carried out based on the method described by Bender et al. (2017): Frozen brains were cut horizontally into 25 μm thin sections with the cryotome. Sections containing EC were first collected in PBS and then processed "free-floating" (i.e., transferred from solution to solution with a metallic hook), because this improves antibody penetration. Processing included: 1) permeabilization with PBS-T for 20 minutes. 2) Blocking of non-specific binding using 3% normal goat serum (in PBS-T) for one hour at room temperature (RT). 3) Incubation with primary antibodies at 4°C

overnight in the blocking solution. Details of the used primary antibodies were listed in Table 2.1.

On the second day, primary antibodies were carefully removed and the sections washed in PBS twice for 10 minutes, followed by incubation with the secondary antibodies (listed in Table 2.2). For immunofluorescence, incubation with the fluorophore-labeled secondary antibodies was carried out in darkness at RT for 3 hours. Sections were then washed again in PBS for 5 minutes and subsequently treated with DAPI (1:100.000) for 1 minute. After another washing step (5 minutes in PBS), sections were carefully mounted on glass slides and dried in the dark, before they were embedded with fluorescent mounting medium (Dako, Cat#S2002) and coverslipped for microscopic inspection. For light microscopy, biotinylated goat anti-rabbit IgGs (1:250) were applied. After incubation with the secondary antibodies, sections were washed in PBS for 5 minutes and then incubated with Avidin-peroxidase complexes according to the manufacturer's instructions (ABC-kit, Vector Laboratories, Cat#PK-6100), before sections were exposed peroxidase substrate (DAB-kit, Vector Laboratories, Cat#SK-4100) at RT until an enzymatic colour reaction (brownish stain) was visible. Sections were then washed in PBS again, carefully mounted on glass slides and dried. Sections were further dehydrated by passing the slides through increasing concentrations of ethanol (50, 70, 95, 100%, 3 minutes each) and xylole (2x 100%, 5 minutes each). Finally, the slides were coversliped with Entellan. Negative-control experiments, omitting primary antibodies, were always performed in parallel.

For immunohistochemistry with slice cultures, cultures from Thy1-eGFP positive pups were cut into 25 µm thin sections with the cryotome. Sections were mounted on glass slides and dried before being processed. Sections from experimentally-treated and vehicle-treated "sister cultures" were always mounted onto the same slide, to optimize comparability. The margins of the sections were marked on the glass slide with a delimiting pen (DAKO, Cat#S2002). Subsequently, sections were post-fixed with 4% PFA for 15 minutes and washed for 5 minutes with PBS in glass jars. Slides were then transferred to a wet chamber

for further processing, following the protocol for immunohistochemistry as described above. Rabbit anti-GFP (1:1000, see Table 2.1) and the corresponding secondary antibody, anti-Rabbit Alexa Fluor 488 (1:500, see Table 2.2), were used.

2.3.4 Electron Microscopy

For EM, organotypic slice cultures were postfixed with 1% OsO4 for 20 minutes after carefully removing the 2.5% glutaraldehyde from the plates. In order to avoid tissue damage by water retention, slices were subsequently dehydrated in graded alcohol (35%, 50%, 70%, 96%, 100%, 100%; at least 10 minutes each), propylene oxide (twice, each for 10 minutes) and Epon (2 hours at RT). Each specimen (tissue cultures) was covered with a drop of Epon on a silicone plate, then covered by a film and incubated in the oven at 68°C overnight. On the next day, capsules filled with Epon were placed, each on one slice, on the film. When slices were all covered by capsules, they were kept in the oven again at 68°C overnight.

Tissue blocks were then trimmed to contain only CA1. They were first cut into 1 µm-thin sections on a microtome with a diamond knife, and sections were stained with toluidine blue / pyronine. The dye made the structure of the tissue well recognizable and thus permitted orientation under light microscope. Finally, blocks were cut into 100nm-ultrathin sections with an ultramicrotome, and the sections, including CA1, were placed on grids. For contrasting, sections were exposed to uranyl acetate, followed by lead citrate.

Electron micrographs were taken from CA1 SLM, defined as the area above the hippocampal fissure, with a magnification of 2950x by a transmission electron microscope (CM 100, Philip). 10 pairs of consecutive pictures were taken from each slice. Areas with large dendrites or blood vessels were avoided. To avoid bias, the EM pictures were taken by a technician who did not know the design of the project. The technician subsequently "coded" each picture to make sure that my synapse counting was performed "blindly".

2.3.5 Western Blot

2.3.5.1 Protein extraction from tissue

For Western Blot analyses, deep-frozen hippocampus or EC tissue from mice, or organotypic cultures, which were experimentally- or vehicle-treated ("sister cultures"), were subjected to protein extraction. As for the organotypic cultures, the protein amount received from one single tissue culture was too low, all equally-treated cultures from one pup (usually 4-7) were pooled together for analysis. Thus, the "n" in the Western Blot analyses represents the number of pups used, and not the number of pairs of individual "sister slices", as in other experiments (e.g., EM, spine counts).

For protein extraction, the samples were thawed and homogenized with RIPA buffer according to the weight of the tissue. The RIPA buffer was supplemented with a mixture of proteinase inhibitors before use. After incubation on ice for 40 minutes, the samples were centrifuged at 13.000 rcf for 30 minutes at 4°C. The supernatant was collected, quick frozen in nitrogen and stored at -80°C.

2.3.5.2 Bradford protein assay

The Bradford protein assay (Bradford, 1976) was carried out to determine the concentrations of protein. The method is based on the properties of the anionic dye Coomassie Brilliant Blue in acidic solution. The dye forms complexes with protein and thus in turn has the absorption spectrum maximum at 595 nm. The increase in the absorption peak of the dye at 595 nm is proportional to the amount of dye molecules bound to the protein and is therefore proportional to the amount (concentration) of protein in the sample. Briefly, a standard curve of 0, 1.25, 2.5, 5, 7.5, 10 µg/µL Bovine Serum Albumin (BSA) was applied. 1 µL RIPA buffer was added to each standard probe in order to eliminate its potential influence on the calculation. Of the sample probe, 1 µL was diluted in 20 µL distilled water. 1 mL reagent (1 portion Bio-Rad protein assay mixed with 4 portions distilled water) was added to each standard and sample probes, dye binding was subsequently measured

by the Bio-photometer (Eppendorf, Germany) and the corresponding protein concentrations were determined.

2.3.5.3 SDS-Page

Sodium Dodecyl Sulfate polyacrylamide gel electrophoresis (SDS-Page), developed by Laemmli (1970), is commonly used to separate the protein mixtures depending on molecular weight in the electric field. In the experiments of my thesis, 0.75 mm-thick 10% and 12% separating gels (protocol see Table 2.3) were used and 30 µg of protein was applied. If necessary, protein samples were diluted with distilled water according to their concentrations determined by the Bradford assay, to equivalently adjust the volumes of all samples in one gel. Identical volumes of 5x Laemmli sample buffer mixed with dithiothreitol (DTT) were then added to each sample probe. The mixture was denatured at 95°C for 5 minutes to linearize the protein for reliable separation. 5 µL PageRuler™ Prestained protein ladder was used as the size marker. The gel was first run at the voltage of 80V in the stacking gel for around 30 minutes and then at 120V in the separating gel for about 1 hour, i.e., until the anionic dye bromophenol blue (BPB) ran out of the gel.

	10% Separating gel	12% Separating gel	Stacking gel
H2O	8 mL	6.6 mL	5.5 mL
Acrylamid 30%	6.6 mL	8 mL	1.7 mL
1.5 M Tris PH 8,8	5 mL	5 mL	-
0.5 M Tris PH 6,8	-	-	2.5 mL
10% SDS	200 µL	200 µL	100 µL
BPB	-	-	100 µL
10% APS	200 µL	200 µL	100 µL
TEMED	8 µL	8 µL	10 µL

Table 2.3: Recipes for four 0.75mm polyacrylamide gel

2.3.5.4 Blotting

In order to detect the target proteins, the proteins were blotted on a nitrocellulose (NC) membrane after gel electrophoresis. The proteins could migrate from the acrylamide gel onto the NC membrane without disturbing the organization they had in the gel. At the

constant voltage of 100V, the proteins were blotted for 90 minutes followed by staining with Ponceau S to check the quality of the blotting.

2.3.5.5 Immunodetection

Membranes were cut into horizontal stripes according to the molecular weight of the target proteins. For instance, a membrane blotted from the 10% gel could be cut roughly at the level of 26 kDa, 34 kDa, 72 kDa, 95 kDa or 130 kDa marker bands in order to specifically detect SNAP25 (25 kDa), GAPDH (36 kDa), GPER1 (55 kDa), PSD95 (95 kDa) and spinophilin (130 kDa), respectively. Membrane stripes were incubated with either 5% non-fat milk solution (GAPDH, β-actin, GPER1, spinophilin, SNAP25, n-cofilin) or 5% BSA solution (ITPKA, PSD95, p-cofilin) for 1 hour to block nonspecific binding sites. The primary antibody was diluted in the corresponding blocking solution. The membranes were incubated at 4°C with primary antibody in the shaker overnight. It should be noted that for loading control β-actin was used in the development time course analyses, whereas GAPDH was used in all other experiments. On the second day, membranes were washed with PBS-Tween (3x 10 minutes) and incubated with secondary antibodies at RT for 1 hour. Subsequently, they were washed again with PBS-Tween (3x 10 minutes).

For quantitative detection of the proteins on NC membranes by chemiluminescence, two different types of chemiluminescent HRP substrates (ECL and Immobilon Western [Millipore]) were used. The ECL substrate was used to detect GAPDH (approx.1min), β-actin (approx.1 min), n-cofilin (approx.1-2 min), GPER1 (approx.1min) and SNAP25 (approx. 40 s) while the Millipore substrate was used for ITPKA (approx.30 s), PSD95 (approx.3-5 min), p-cofilin (approx.3-5 min), spinophilin (approx.2-3 min). The signal was visualized by FUSION-SL4 advanced imaging system.

2.4 Quantification and Statistical analysis

2.4.1 Analysis of dendritic spine in organotypic culture of Thy1-eGFP mice

For orientation, overview pictures of entorhinal-hippocampal sections were captured on the Keyence BZ9000 fluorescence microscope with a 20x objective (Figure 2.1A). If the structure of the hippocampus was well preserved and eGFP-staining of pyramidal neurons in CA1 was clearly visible, sections were taken to a Leica SP8 confocal microscope and images were acquired using 63x oil objective with 6x zoom (settings: 2048*512 pixels, 0.1 µm z-steps, 66.6 px/µm resolution). From each slice, five dendrites were selected for further analysis. To make sure that they belong to CA1 SLM, they were chosen from an area near the hippocampal fissure. Fiji (ImageJ) software (National Institutes of Health) was used for spine analysis. Sequence images were first converted to 8-bit gray value images. The plugin "Neurite tracer" was applied to trace and measure the length of the dendrites. Spine counting was done manually and the results from each of the five dendrites was added up to generate one representative value per slice (i.e., slice equaling n=1). Dendritic spines were further classified as follows: non-stubby (spines with a neck) and stubby (protrusions devoid of a neck). As referred before in section 2.4, the observer was blinded to the experimental group.
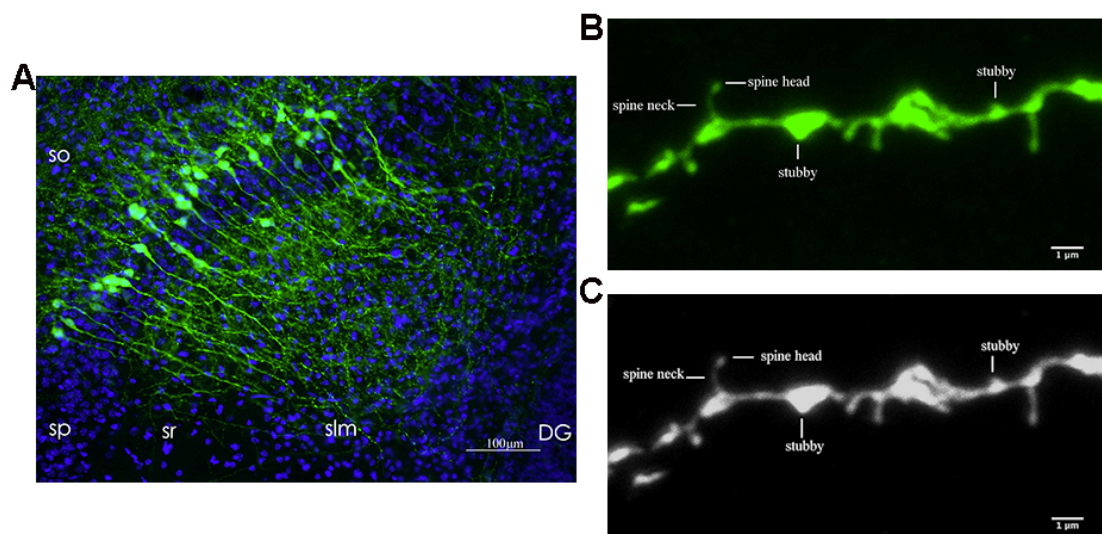
Figure 2.1: Images of dendrites and dendritic spines in an organotypic culture from a Thy1-eGFP mouse. (A) Image showing eGFP-labeled pyramidal neurons in CA1 of a slice culture from a Thy1-eGFP-mouse (captured by Keyence BZ9000; scale bar: 100 µm); (B) Example of a dendrite in CA1 SLM, as chosen for analysis. Dendritic spines are recognized as "stubby" or "non-stubby" (captured by Leica SP8 confocal microscopy; scale bar: 1 µm); (C) The same dendrite as in (B) represented as a gray-value image, converted by Fiji Software (scale bar: 1 µm).

2.4.2 Analysis of spine synapse density

Spine synapse density was analyzed using electron micrographs. Only asymmetric synapses on spines were considered. Symmetric synapses and synapses on dendrite shafts were excluded from the analysis. The following criteria were used to define an asymmetric spine synapse: (1) visible presynaptic membrane, (2) presynaptic vesicles in the bouton, (3) synaptic cleft, (4) postsynaptic membrane with postsynaptic density (see Figure 2.2).
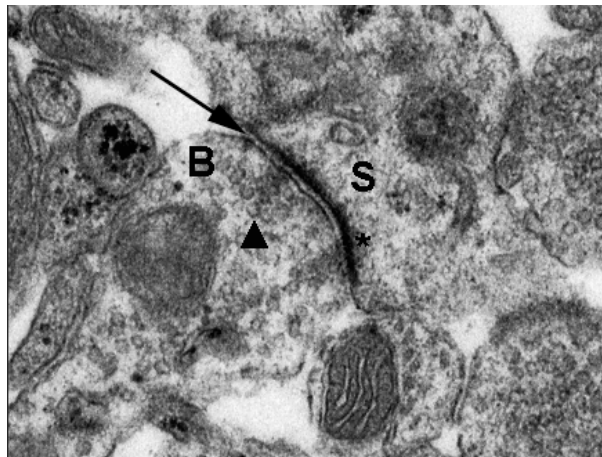
Figure 2.2 Electron micrograph showing an asymmetric spine synapse (S: spine, *: postsynaptic density, B: bouton, ↑: synaptic cleft, ▲: vesicle)

The disector technique (Sterio, 1984) was used for counting. Briefly, always two consecutive pictures covering corresponding neuropil were analyzed. The first picture is considered the "reference picture", whereas the second picture serves as the "look-up picture" (Figure 2.3). All synapses that are recognizable in only one of these two pictures, but not those which are present in both pictures, were positively counted. Subsequently, a reference square (8 µm * 8 µm) was placed on the image at a defined position. All spine synapses in this reference square were included in the evaluation
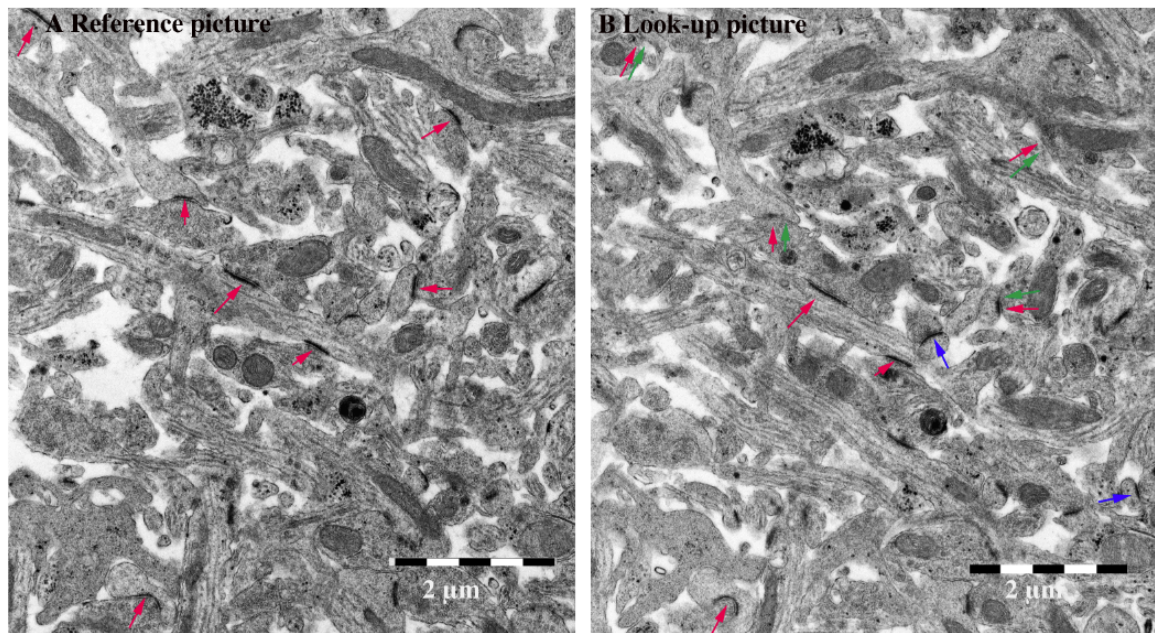
Figure 2.3 Two consecutive electron micrographs covering corresponding neuropil. (A) Reference picture (red arrows indicate spine synapses). (B) Look-up picture (blue arrows indicate newly found spine synapses; green arrows indicate spine synapse sites from the "reference picture", where synapses had disappeared). Only those spine synapses that appeared in only one of the pictures (i.e., blue and green arrows) were included in the count. Scale bar: 2 μm.

2.4.3 Quantitative western blot analysis

The open access software "Fiji" was used for quantitative analyses of target proteins. Briefly, the images were all converted to 8-bit gray value pictures first. Then, the gray intensity of each band was calculated, representing the protein expression. All target protein (GPER1, spinophilin, SNAP25, ITPKA, PSD95, n-cofilin, p-cofilin) values were normalized by division to the corresponding loading control (GAPDH or β-actin) values. Because virtually identical "sister cultures" were used for the analysis of G1-effects in slice cultures, the values from the control cultures were set at 100% and the values from the experimentally-treated cultures were calculated in relation to them. Data are therefore presented as "% of control".

2.4.4 Statistical analysis

Statistical analysis was performed with Prism 7.0a (GraphPad, San Diego, CA, USA). All data are presented as mean ± standard error of mean (SEM). For unpaired data (expression analyses in mouse brain tissue), "Mann–Whitney test" was used. For paired data that

resulted from the comparison of "sister cultures" (G1- and E2-effects on spine density, G1-effects on spine synapse density), data were first examined for "normal distribution" using "Kolmogorov-Smirnov test", and, if the data were normally distributed, "paired t test" was applied. If the data were not normally distributed, the nonparametric "Wilcoxon matched pairs signed rank test" was used. For changes in synaptic protein, examined by western blot analysis, "Wilcoxon signed rank test" was applied, as the control group was normalized to 100% and all other values were calculated in relation to them. P $<$ 0.05 was considered significant.

3. Result

3.1 GPER1 expression in Hippocampus and EC

In preparation for the study, I first determined expression levels of GPER1 in hippocampus and EC using Western Blot analyses. Western Blots using GPER1 antibodies from Abcam (see "Methods") regularly revealed a single band at the height of approximately 55 kDa, which according to published data (Meseke et al., 2018; Zhao et al., 2018) corresponds to the size of GPER1 (Figs: 3.1 and 3.2).

3.1.1 Developmental time course of GPER1 protein expression in female mouse hippocampus

In order to describe developmental time course changes, hippocampal tissue from female mice of different ages was processed (P3, P10 and P17, n=3 each). The analysis revealed a steady increase of signal intensity for GPER1 in female hippocampal tissue, suggesting that expression is relatively low at P3, but has reached substantial levels already at P10 and further increases to the age of P17 (Figure 3.1).
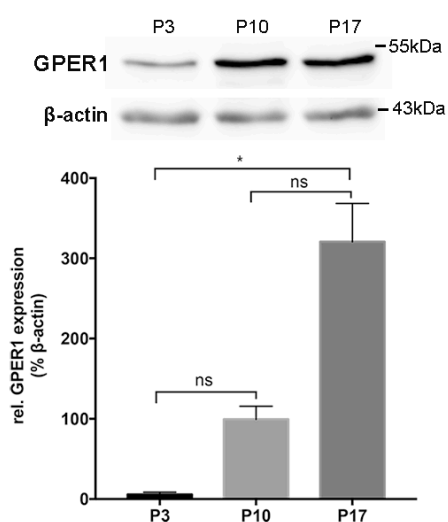
Figure3.1: Development time course of GPER1 expression in the hippocampal of female mice.

Note: Expression of GPER1 increased with postnatal development (P3 vs. P10: p=0.54, P3 vs. P17: p=0.02, P10 vs. P17: p=0.54; n=3 for each age; Dunn's multiple comparisons test). Data are normalized to the expression of β-actin.

3.1.2 Comparison of GPER1 protein expression in female and male mice

In addition, GPER1 protein expression was compared in hippocampal and EC tissue from male and female mice at ages that were relevant for the concept of the study: P13, which is age-equivalent to the organotypic cultures used for analysis (Figs. 3.2 A, B) and P56, which was considered "adult". At both ages, similar GPER1 expression was observed in the male and female tissue (Figs. 3.2 C, D). Taken together, these analyses (3.1.1 and 3.1.2) suggest that substantial GPER1 levels are already expressed in the developing hippocampus and EC, and that levels do not significantly differ between sexes.
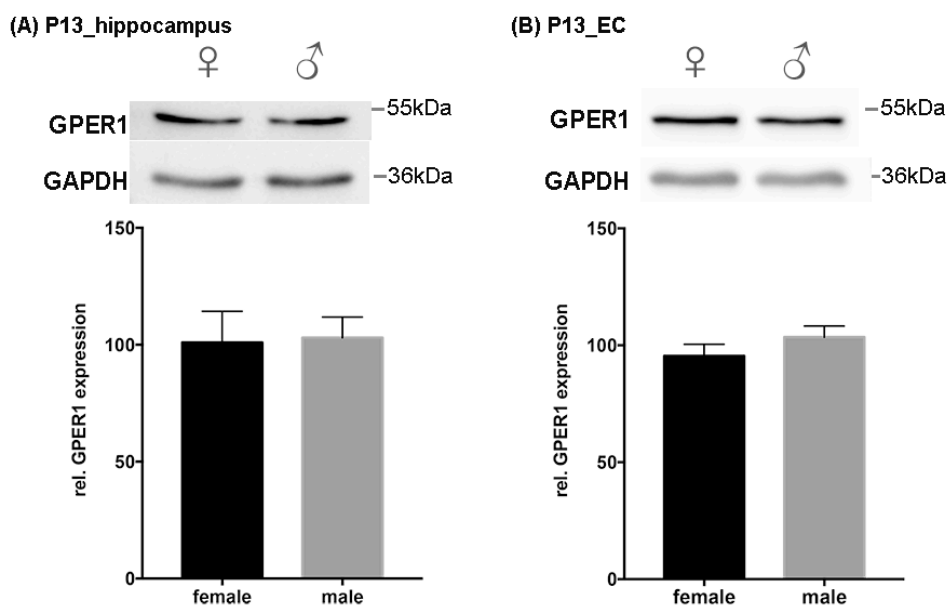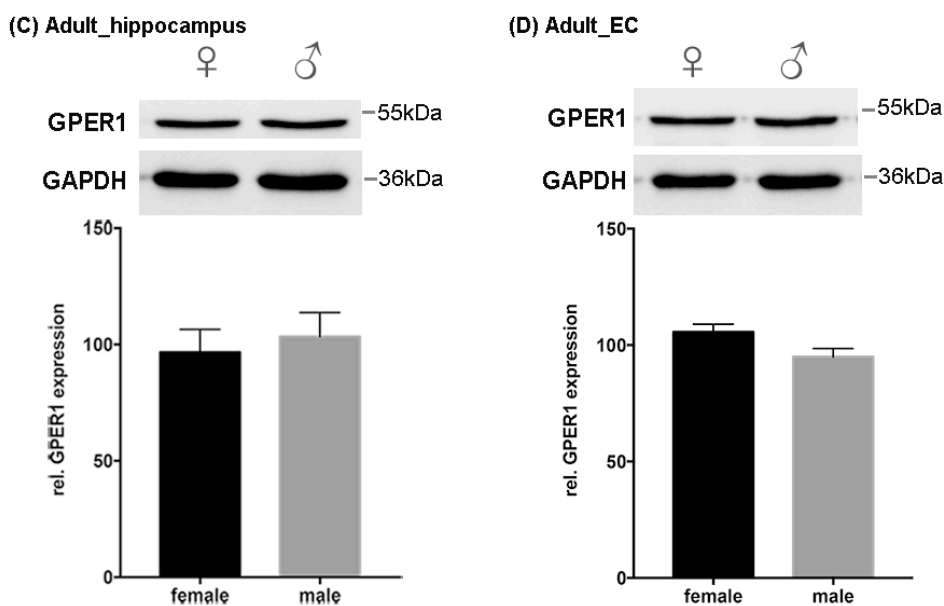
Figure 3.2 Comparison of GPER1 expression in male and female hippocampus and EC. (A) Immunoblots and quantification of GPER1 expression in the hippocampus of P13 mice (rel. expression of GPER1: 101±13% in females vs 103±9% in males, p=0.82, n=6 of each sex; Mann-Whitney tests); (B) Immunoblots and quantification of GPER1 expression in the EC of P13 mice (rel. expression of GPER1: 96±5% in females vs 104±5% in males, p=0.42, n=6 of each sex; Mann-Whitney tests) ; (C) Immunoblots and quantification of GPER1 expression in hippocampus of P56 mice (rel. expression of GPER1: 97±10% in females vs 103±10% in males, p=0.7, n=3 of each sex; Mann-Whitney tests); (D) Immunoblots and quantification of GPER1 expression in EC of P56 mice (rel. expression of GPER1: 106±3% in females vs 95±4% in males, p=0.2, n=3 of each sex; Mann-Whitney tests). Data are normalized to GAPDH. No significant difference was observed between sexes.

3.1.3 GPER1 expression in hippocampus, determined by immunohistochemistry and immunofluorescence

Immunohistochemistry (Figs. 3.3 A-C) and immunofluorescence (Figs. 3.3 D-F) were used to characterize the expression patterns of GPER1 in hippocampus and EC. Both adult and adolescent (P13) mice were used in these studies. In hippocampus, GPER1 expression was particularly strong in area CA1, localizing to pyramidal cell somata and to the apical dendritic field. Interestingly, in the dendritic field, expression was much higher in the stratum-lacunosum-moleculare (SLM), comprising the distal apical dendrites of the pyramidal cells, compared to stratum radiatum (SR), which comprises the proximal dendrites (Figs. 3.3 A, B and D, E). This observation is consistent with previous findings in

mouse (Waters et al., 2015) and rat (Meseke et al., 2018), and suggests that functions of GPER1 may be specifically associated with afferents that terminate in SLM, including axons of the temporoammonic path (TA). Patterns of GPER1 expression were largely identical in adult and adolescent mice (compare Figs. 3A and B, 3D and E), and were not dependent on the sex of the animals. Negative-control experiments, omitting primary antibodies, were always performed in parallel, and no immunoreactivity was detected (Figs. 3.3 C)

.
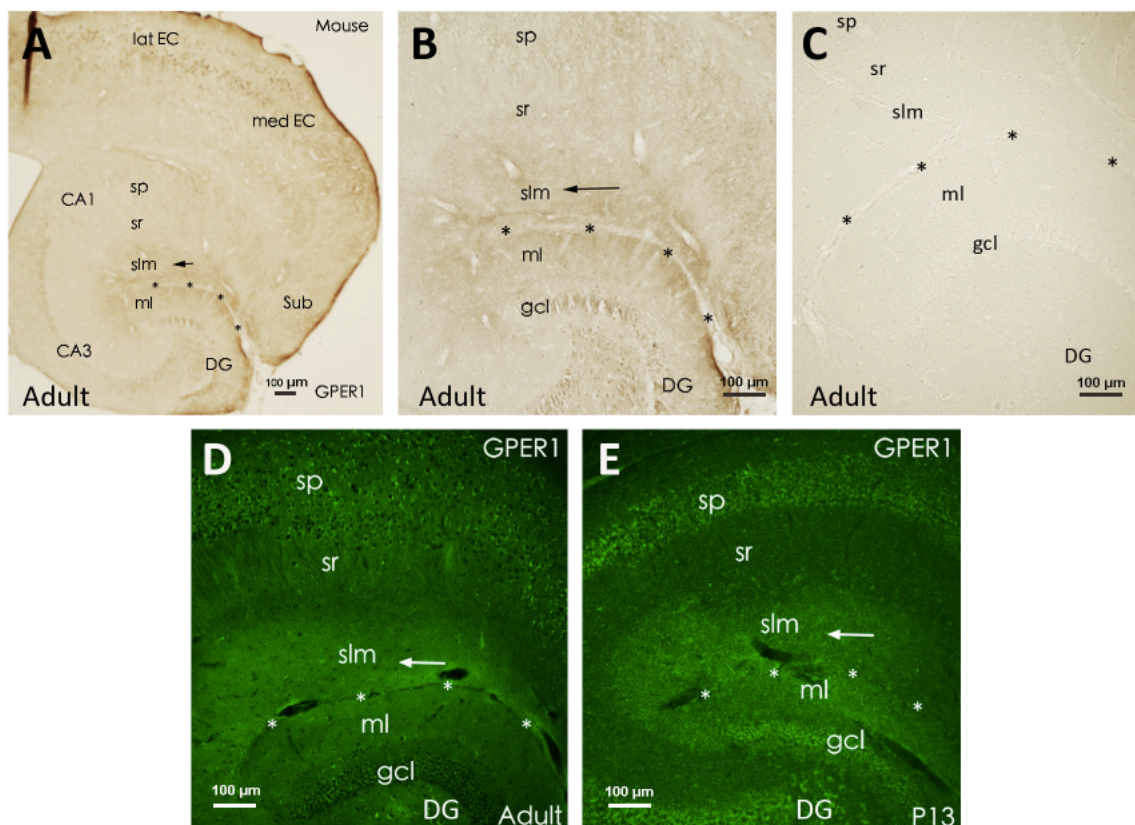
Figure 3.3 Expression of GPER1 in hippocampus and EC of female mice. (A, B) Using the DAB-method, GPER1 immunostaining is recognizable in hippocampus and EC in adult mouse both at low (A) and high magnification (B). The high magnification view (B) illustrates a prominent immunoreactivity in CA1 SLM (arrow) and in the outer third of dentate gyrus ML. (D, E) This pattern is also recognizable, if immunofluorescence is used for GPER1-detection, both in adult (D) and immature (P13, E) mouse hippocampus. (C) No immunosignal was detectable when the first antibody was omitted. Scale bar: 100 μm.

3.2 Analysis of dendritic spine density in SLM of Thy1-eGFP-mice

3.2.1 Effects of G1-treatment on spine density in SLM

Prompted by the observation illustrated in Figure 3.3 that GPER1-expression is particularly prominent in CA1 SLM, I next wanted to know what its function at this position could be. As a well-known function of E2 is the regulation of spine density in hippocampus (Mukai et al., 2007; Srivastava et al., 2008; Hasegawa et al., 2015), including SLM (Smith et al., 2016), I opted to first study whether GPER1 contributes to this type of neuroplasticity. For this purpose, I used organotypic entorhinal-hippocampal slice cultures, prepared from Thy1-GFP transgenic mice (Feng et al., 2000a), which express GFP within selected pyramidal cells in hippocampal CA1 and thus render their dendrites and dendritic spines clearly visible (see Figure 2.1., in the "Methods"). To focus specifically on the effects of GPER1, cultures were treated with the GPER1-agonist G1 (or vehicle), which was added at DIV4 and then incubated for 24 or 48 hours (details see section 2.3.2). After fixation, pictures were taken from dendrites in SLM with a confocal microscope, and numbers of dendritic spines per area were determined. Most of the spines observed were immature spines, and fully mature spines (mushroom spines) were randomly seen, which was not unexpected, as the equivalent age of the cultures is about P13. Therefore, I classified the spines as "non-stubby" (spines with a neck, which are considered to be in a state of progressed maturation) and "stubby" (protrusions devoid of a neck, which are considered immature spines in *statu nascendi*; Harris et al. 1992.).

The analysis revealed that G1 had indeed a regulatory effect on the spine density in CA1 SLM, as both after 24 hours (Figure 3.4A) and after 48 hours (Figure 3.5A), numbers of non-stubby (i.e., more mature) spines were significantly elevated after G1-treatment. However, surprisingly, this effect was only seen, if female tissue was analyzed (red bars), whereas dendritic spine density was unchanged in SLM in the cultures from males (blue bars). When the non-stubby spines were also included in the analysis, a significant effect still persisted in the female tissue after 24 hours (Figure 3.4B), whereas only a tendency

was seen after 48 hours (Figure 3.5B). Taken together, these findings suggest that G1 has a sex-specific effect on spine density in SLM.
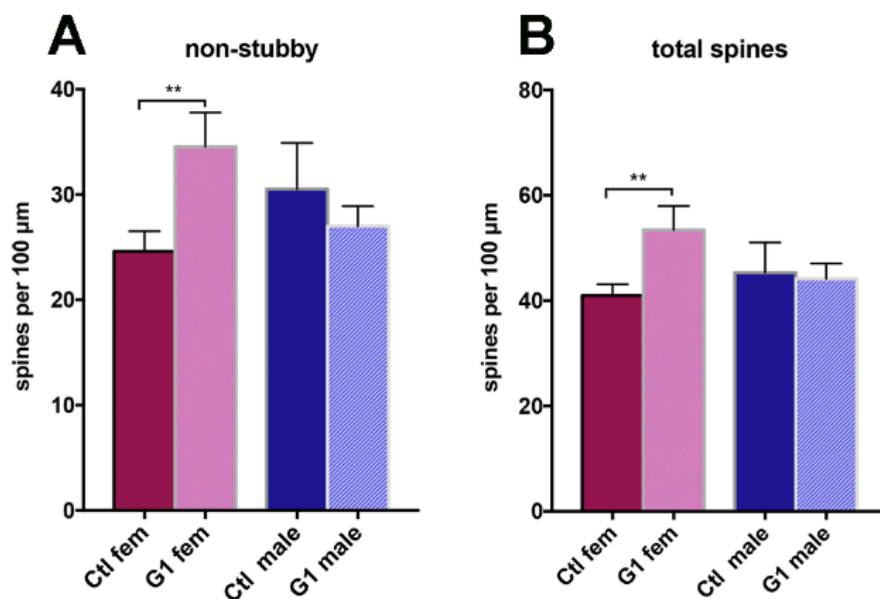
Figure 3.4 Changes of dendritic spine density in SLM after treatment with G1 for 24 hours. (A) For the non-stubby spines, G1-treatment caused a significant increase relative to vehicle-treated controls in females (red bars: control: 24.6±1.92, G1: 34.54±3.26 spines per 100 µm; p=0.0081, n=10; paired t-test), but not in males (blue bars: control: 30.5±4.41, G1: 27.01±1.89 spines per 100 µm; p=0.28, n=10; paired t-test). (B) Similarly, total spine density, including the stubby spines, was significantly altered in the females (red bars; control: 41±2.14, G1: 53.45±4.50 spines per 100 µm; p=0.0055, n=10; paired t-test), but not in males (blue bars; control: 45.32±5.72, G1: 44.17±2.90 spines per 100 µm; p=0.80, n=10; paired t-test).
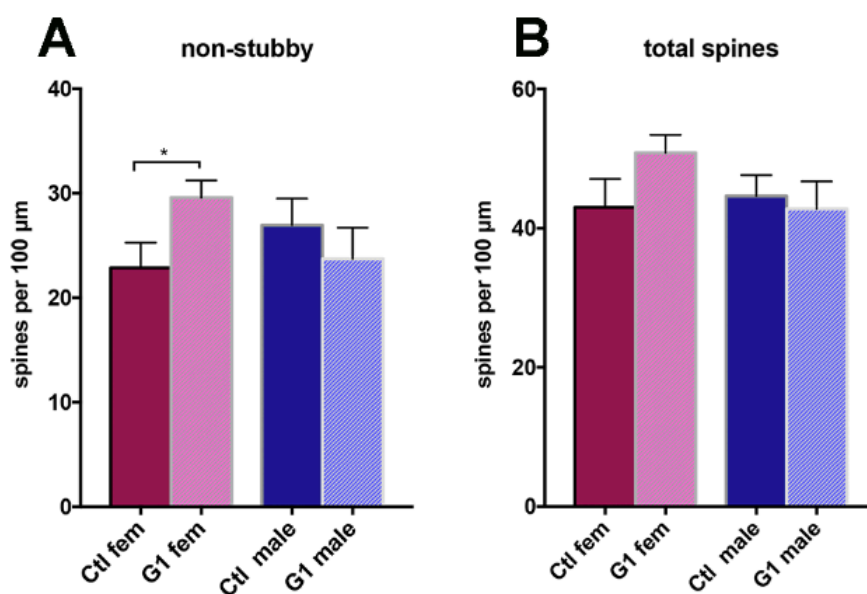
Figure 3.5 Changes of dendritic spine density in SLM after treatment with G1 for 48 hours. (A) As after 24 hours, non-stubby spine density was significantly increased in females (red bars: control: 22.87±2.40, G1: 29.59±1.64 spines per 100 µm; p=0.035, n=10; paired t-test), but not in males (blue bars: 26.95±2.54, G1: 23.73±2.98 spines per 100 µm; p=0.35, n=10; paired t-test). (B) Total spine density, including the stubby spines, showed a slight, but non-significant, trend towards an increase (red bars: control: 42.99±4.09, G1: 50.83±8.16 spines per 100 µm; p=0.15, n=10; paired t-test), whereas no evidence of a change was observed in the males (blue bars: control: 44.62±3.023, G1: 42.79±3.93 spines per 100 µm; p=0.6769, n=10; paired t-test).

3.2.2 Effects of E2-treatment on spine density in SLM

So far, only few studies have focused on estrogen effects on spines in CA1 SLM and no *in vitro* experiments have yet directly shown modulation of E2 on TA-CA1 synapses. Therefore, and because the effects of G1-treatment shown above could have resulted from so far unknown functions of the G1-compound which are unrelated to estrogen binding, I next repeated the culture experiments applying E2 for 48 hours in low concentration (2 nM), according to Mukai et al. (2007).

Indeed, as shown in Figure 3.6, dendritic spine density was significantly increased after E2-treatment compared to vehicle-treatment, similarly to what was seen after G1-treatment (Figure 3.5). Again, only female tissue responded to the treatment, after which significant differences were observed both among the non-stubby spines only (Figure 3.6A) and if the stubby spines were included (Figure 3.6B). In contrast, no effect of treatment was seen in the tissue from males.
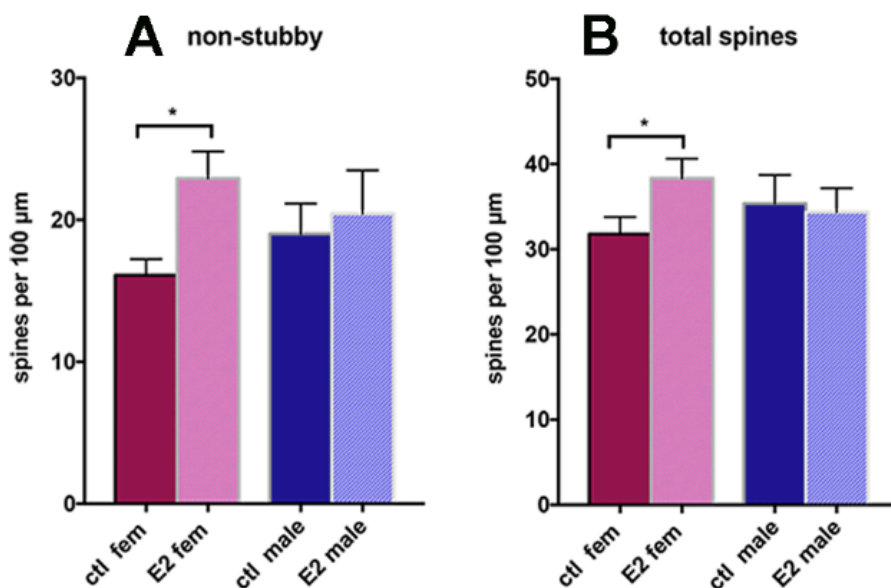
Figure 3.6 Changes of dendritic spine density in SLM after treatment with E2 for 48 hours. (A) For the non-stubby spines, E2-treatment caused a significant increase relative to vehicle-treated controls in females (red bars: control: 16.1±3.19, E2: 22.92±5.39 spines per 100 µm; p=0.030, n=8; paired t-test), but not in males (blue bars: control: 19.01±4.81, E2: 20.43±6.87 spines per 100 µm; p=0.64, n=5; paired t-test). (B) Similarly, total spine density, including the stubby spines, was significantly altered in the females (red bars; control: 31.78±5.70, E2:38.33±6.52 spines per 100 µm; p=0.025, n=8; paired t-test), but not in males (blue bars; control: 35.35±7.52, E2: 34.36±6.33 spines per 100 µm; p=0.74, n=5; paired t-test).

3.3 Analysis of spine synapse density in SLM by electron microscopy

Studies from our laboratory (Kretz et al., 2004; Bender et al., 2010; Zhou et al., 2010; Vierk et al., 2012) and from others (Gould et al., 1990; Woolley et al., 1997; Leranth and Shanabrough, 2001) have firmly established that E2 is involved in the regulation of synapse formation, and particularly of excitatory spine synapses, in hippocampus. In CA1, most of these studies have focused on the stratum radiatum (SR), and only few have analyzed synapse densities in SLM, although E2 may be a critical regulator of synapse density in SLM as well (Smith et al., 2016). This is also suggested by the data presented above (Figs. 3.4 - 3.6) showing that E2 promotes spinogenesis in CA1 SLM, which is likely mediated via GPER1. Thus, I next addressed the question, whether GPER1 activation promotes not only spino-, but also synaptogenesis. For this purpose, I used electron microscopy to analyze

spine synapse densities in organotypic entorhino-hippocampal slice cultures that were treated with G1 (or vehicle) for 24 hours or 48 hours.

The data did not reveal evidence supporting an effect of GPER1 on synaptogenesis in the chose experimental paradigm. Generally, numbers of spine synapses were low in SLM of the organotypic cultures, which is likely due to the fact that the cultures were prepared at an immature stage, when only few temporoammonic path (TA) synapses have yet formed. Additionally, some of the TA fibers have been cut during preparation and may not have had enough time to re-grow into their target area. Nevertheless, numbers of distinct spine synapses were substantial enough to be counted and analyzed (see Figs. 2.2 and 2.3). However, this counting did not reveal any significant differences between G1- and vehicle-treated cultures both after 24 hours (Figure 3.7A) or 48 hours (Figure 3.7B), not even in the female group, in which it was expected. This suggests that the effect of G1-treatment on spinogenesis in the females, as shown above, is not correlated with enhanced synaptogenesis.
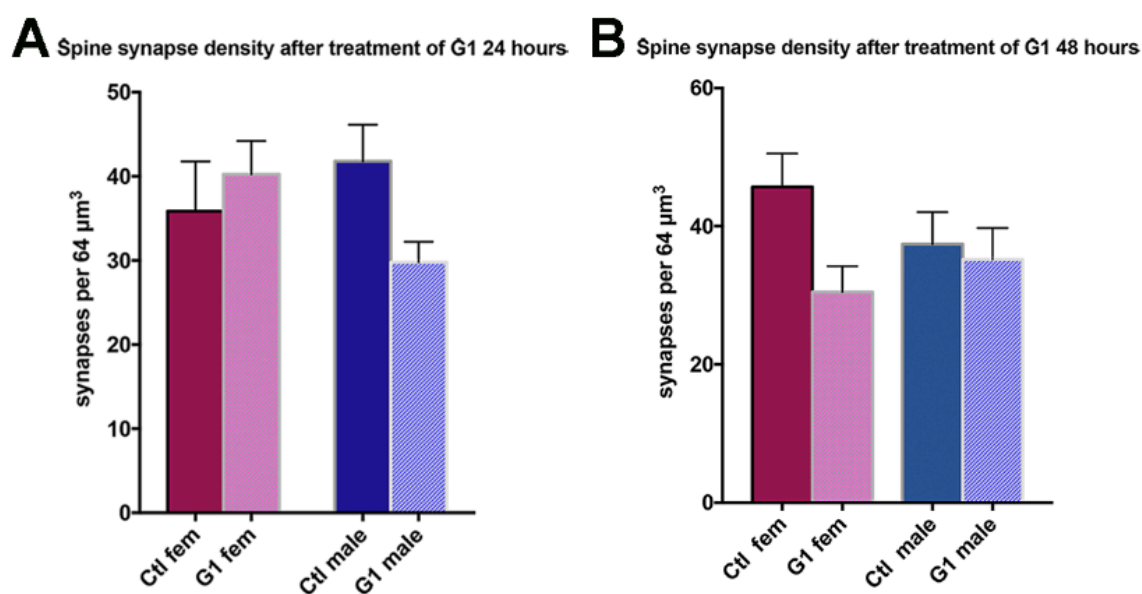
Figure 3.7: Changes in spine synapse density after treatment with G1. (A)After G1 treatment for 24 hours, spine synapse density was slightly higher compared to controles in the cultures from females (red bars: control: 35.88±5.89, G1: 40.25±3.98 synapses per 64 μm^3; p=0.51, n=8; paired t-test), and appeared to be decreased in those from males (blue bars: 41.8±4.33, G1: 29.8±2.47 synapses per 64 μm^3; p=0.092, n=5; paired t-test), but none of these differences were statically

significant. (B) Similarly, after G1 treatment for 48 hours, there was no significant change compared to controls detectable in the cultures from females (red bars: control: 45.67±4.84, G1: 30.5±3.70 synapses per 64 μm^3; p=0.054, n=6; paired t-test) or males (control: 37.40±4.63, G1: 35.2±4.55 synapses per 64μm^3; p=0.81, n=5; paired t-test).

3.4 Changes in synaptic protein expression *in vitro* after stimulation with G1 or E2

3.4.1 Effects of G1 treatment on synaptic protein expression

Changes in spine and synapse morphologies are correlated with changes in the expression levels of synaptic proteins. Concluding from the data presented above (section 3.2), I therefore hypothesized that sex-specific expression changes of synaptic proteins should be detectable in the organotypic cultures after treatment with G1. This was examined by determining expression changes induced by G1 in the total culture lysate for the postsynaptic proteins PSD95, inositol-1,4,5-trisphosphate 3-kinase-A (ITPKA) and spinophilin, as well as for the presynaptic protein SNAP25, because GPER1 may also localize to presynaptic terminals (Waters et al., 2015). In addition, the actin-modulating protein cofilin (n- and p-cofilin) was included into the analysis. Results are listed below:

3.4.1.1 SNAP25

SNAP25 belongs to the SNARE complex family and is important for the neurotransmitter release at the terminal. It controls the exo/endocytic processes by modulating calcium channel subunits (Antonucci et al., 2016). In Western blot analysis, the band is regularly recognizable at about 25 kDa according to its molecular weight (Figure 3.8).

While I hypothesized that presynaptically localized GPER1 could modulate the expression of SNAP25, if activated by G1, this hypothesis was not supported by the data. Quantitative evaluation of the protein in lysate of G1-treated female cultures did not reveal a significant difference of SNAP25 expression relative to the control group, neither after 24 hours (G1: 123±14% of controls), nor after 48 hours incubation with G1 (G1: 94±13% of controls).

Similarly, in male cultures, SNAP25 expression was not significantly altered after G1 treatment.
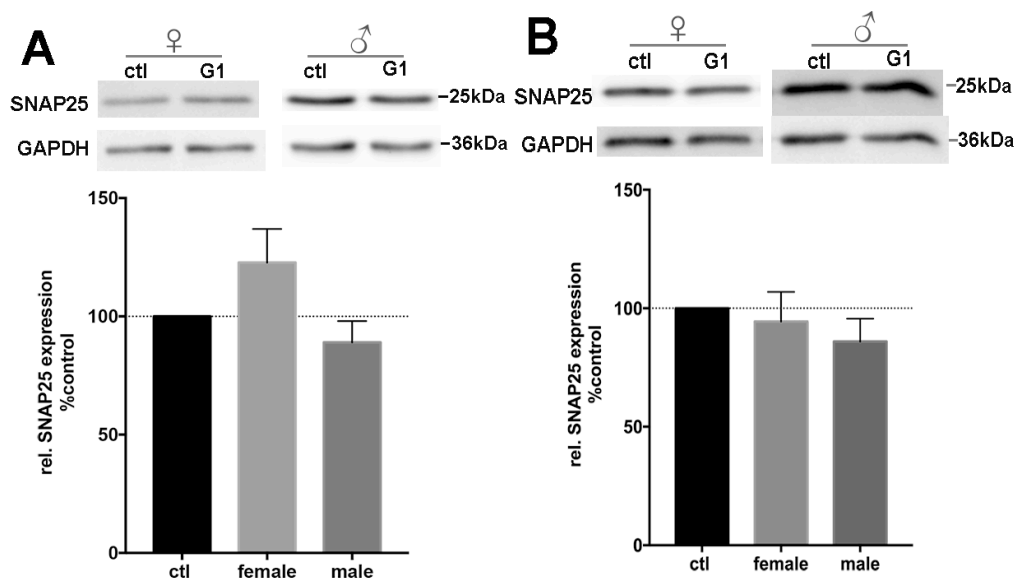
Figure 3.8 Immunoblots and quantification of SNAP25 expression by western blot analysis after G1-treatment in slice culture. (A) Application of G1 for 24 hours: Although SNAP25 expression appeared to be enhanced in female tissue, analysis did not reveal a significant increase (123 ± 14% of the controls, p=0.15, n=12). Expression levels were also not changed in males (89 ± 9% of the controls, p=0.27, n=12; paired t-test). (B) Similar results were observed after 48 hours. No significant changes were detected (females: 94 ± 13% of the controls, p=0.45, n=15 vs. males: 86 ± 10% of the controls, p=0.16, n=14; paired t-test). Data are normalized to GAPDH and related to control expression which was set at 100%.

3.4.1.2. Spinophilin

Spinophilin, also named neurabin-II, is abundant in dendritic spines. It regulates the formation and function of dendritic spines through interacting with actin and protein phosphatase1 (Satoh et al., 1998; Feng et al., 2000b). Furthermore, its expression is subject to regulation by E2 (Fester et al., 2009), suggesting that it could also be influenced by GPER1-activity. The band is detected at 130 kDa in western blots.

Again, quantitative analysis did not support the hypothesis of an GPER1-mediated effect on spinophilin expression. Expression levels were not significantly different from those in the controls in slice cultures deriving from female or male pups (Figure 3.9).
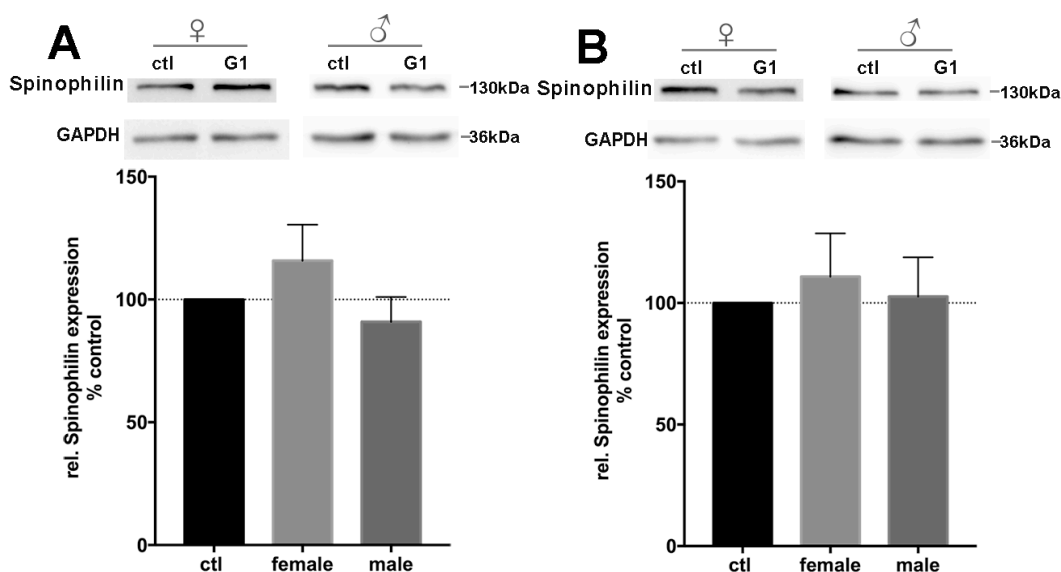
Figure 3.9: Immunoblots and quantification of spinophilin expression by western blot analysis after G1-treatment in slice culture. (A) Spinophilin expression after G1 treatment for 24 hours (females: 116 ± 15% relative to the controls, *p*=0.85, n=12 vs. males: 91 ± 10% relative to the controls, *p*=0.51, n=12; paired t-test). (B) Spinophilin expression after G1 treatment for 48 hours (females: 111±18%relative to the controls, *p*=0.97, n=14 vs. male: 103±16% relative to the controls, *p*=0.97, n=12; paired t-test). No significant changes were detected. Data are normalized to GAPDH and in related to control expression which was set at 100%.

3.4.1.3. ITPKA

ITPKA, the neuronal isoform of the ITPK family, is an actin-bundling protein highly enriched at dendritic spines. It is specifically expressed in the CA1 region and in DG in hippocampus (Mailleux et al., 1993; Köster et al., 2016), and its activity may be regulated by E2 (R.A. Bender, unpublished data). Its molecular weight is 55 kDa.

As for the proteins above, significant effects of G1-treatment on ITPKA-expression were not observed, neither in female slice cultures nor in the cultures from males (Figure 3.10).
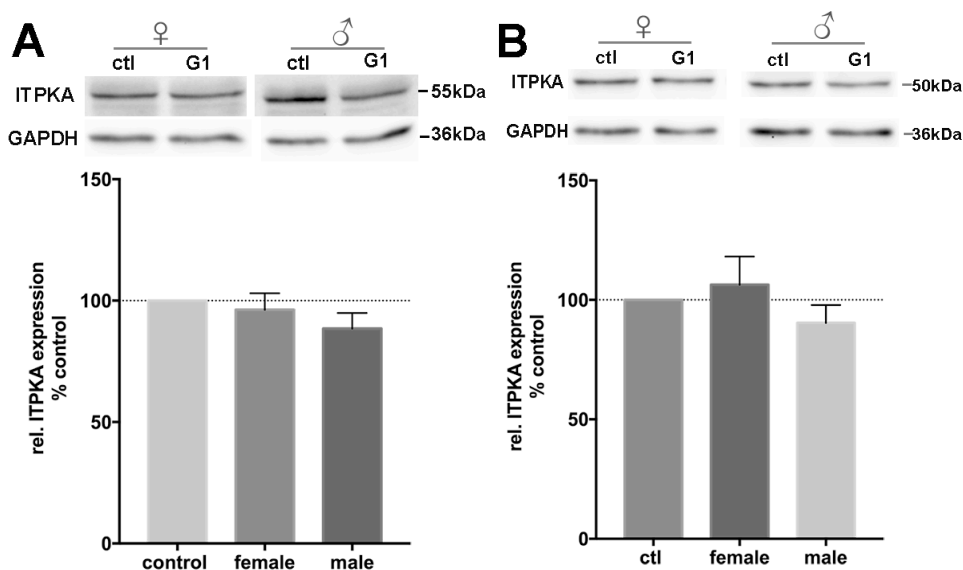
Figure 3.10: Immunoblots and quantification of ITPKA expression by western blot analysis after G1-treatment in slice culture. (A) ITPKA expression after G1 treatment for 24 hours (females: 96 ± 7% of the controls, *p*=0.43, n=11vs. males: 89 ± 6% of the controls, *p*=0.09, n=12; paired t-test). (B) ITPKA expression after G1 treatment for 48 hours (females: 106 ± 12% of the controls, *p*=0.68, n=11 vs. males: 90 ± 8% of the controls, *p*=0.15, n=13; paired t-test). No significant differences were observed. Data are normalized to GAPDH and related to control expression which was set at 100%.

3.4.1.4. PSD95

PSD95 is the most abundant protein in the postsynaptic density (PSD; Cho et al., 1992; Chen et al., 2005), which is defined as the electron-dense accumulation of proteins in the postsynaptic membrane of excitatory synapses, that is visible in EM studies (Broadhead et al., 2016; Figure 2.2). Importantly, it has been shown to be associated with GPER1 in CA1 dendrites and to be regulated by systemically administered G1 *in vivo* (Waters et al., 2015). Its molecular weight is about 95 kDa.

Quantification of PSD95 revealed a significant increase of expression in the lysate of cultures after treatment with G1 for 24 hours, but only if the cultures derived from females (141±17% of the controls; p=0.013, n=11; Figure 3.11A). In contrast, no significant expression changes were observed in cultures deriving from males (94 ± 9% of the controls; p=0.66, n=12; Figure 3.11A). After 48 hours G1 treatment, PSD95-expression in female tissue slices still appeared enhanced. However, the difference was not significant, (129 ± 23% of the controls, p=0.57, n=15 Figure 3.11B). Similarly, in the male cultures, PSD95

expression appeared to be enhanced after 48 hours G1-treatment, without reaching

significance levels (140 ± 23% of the controls; p=0.15, n=12; Fig. 3.11B)
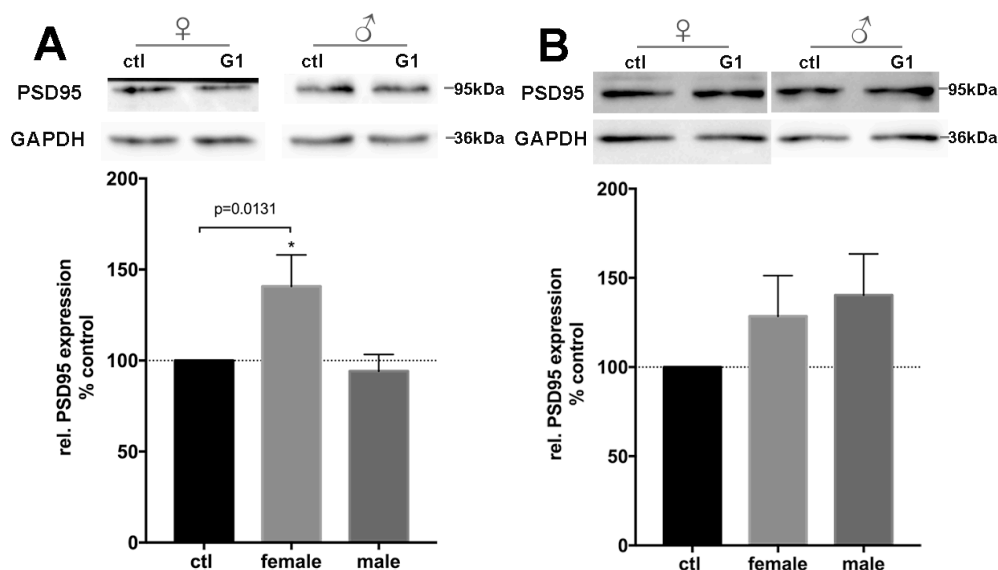
Figure 3.11: Immunoblots and quantification of PSD95 expression by western blot analysis after G1-treatment in slice culture. (A) After G1 treatment for 24 hours, a significant increase of PSD95 expression was observed in females (141 ± 17% of the controls, *p*=0.013, n=11), but not in males (94 ± 9% of the controls, *p*=0.66, n=12; paired t-test). (B) After the treatment of G1 for 48 hours, PSD95 expression levels were not significant different from controls both in females and males (females:129 ± 23% of the controls, *p*=0.57, n=15 vs. males: 140 ± 23% of the controls, *p*=0.15, n=12; paired t-test). Data are normalized to GAPDH and related to control expression which was set at 100%.

3.4.1.5. n-Cofilin and p-Cofilin

Since actin polymerization is a critical factor in the formation of dendritic spines (Matus, 2000), cofilin levels were determined in the organotypic slice cultures derived from P7-8 mice treated with G1. Cofilin dynamically regulates actin filament (F-actin) networks by increasing or decreasing available levels of F-actin, whereby phosphorylation of cofilin (p-cofilin) is required for the assembly of F-actin and unphosphorylated cofilin (n-cofilin) promotes de-polymerization of the filaments to G-actin monomers (Fukazawa et al., 2003). Therefore, both cofilin isoforms were examined in the study using isoform-specific antibodies. Cofilin has a molecular weight of 19 kDa.

Quantification revealed that G1-treatment had sex-specifically affected the expression levels of the cofilin isoforms. Thus, whereas n-cofilin levels were not significantly altered by the treatment in both sexes, p-cofilin levels were significantly reduced after 48 hours G1-treatment specifically in the female slices (females: 47 ± 10% of the controls; *p*=0.002, n=11; males: 108 ± 13% of the controls, *p*=0.47, n=12; Figure 3.12B). However, this effect was not yet seen after 24 hours, when in both sexes the n-cofilin and p-cofilin values were not significantly changed (Figure 3.12B). The G1-effect is further reflected in the p-/n-cofilin ratio, which was significantly reduced after 48 hours treatment in the female slices (Figure 3.12B), suggesting reduced levels of actin-filament in these slices.
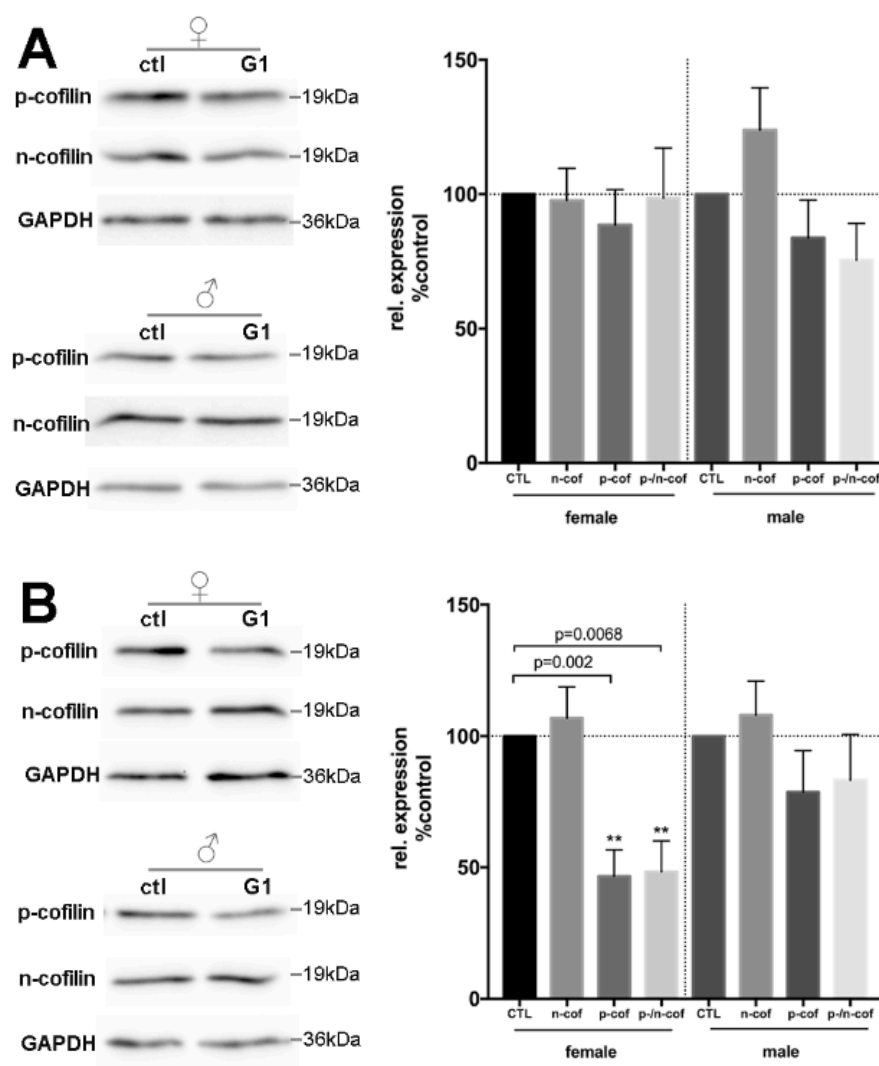
Figure 3.12: Immunoblots and quantification of n-cofilin and p-cofilin expression by western blot analysis after G1-treatment in slice culture. (A) After G1 treatment for 24 hours, n-cofilin and p-cofilin expression was not significantly altered in both sexes (**n-cof:** females: 98 ± 12% of the

controls, p=0.32, n=11 vs. male: 124 ± 16% of the controls, p=0.21, n=11; **p-cof:** females: 89 ± 13% of the controls, p=0.46, n=11 vs. male: 84 ± 14% of the controls, p=0.29, n=11; **p-/n-cof:** females: 99 ± 19% of the controls, p=0.46, n=11 vs. males: 76 ± 14% of the controls, p =0.10, n=11; paired t-test). (B) After G1 treatment for 48 hours, n-cofilin levels were still not different from the controls in both sexes (**n-cof:** females: 107 ± 12% of the controls, p=0.60, n=11 vs. male: 108 ± 13% of the controls, p=0.47, n=12), but p-cofilin levels were significantly reduced specifically in the females (**p-cof:** females: 47 ± 10% of the controls, p=0.002, n=11 vs. male: 79 ± 16% of the controls, p=0.18, n=12). This resulted in a significant reduction of the p-cofilin/n-cofilin ratio specifically in the females (**p-/n-cof**; females: 48 ± 12% of the controls, p=0.0068, n=11 vs. males: 83 ± 17% of the controls, p=0.41, n=12. paired t-test). Data are normalized to GAPDH and related to control expression which was set at 100%.

3.4.2 Effects of E2 treatment on synaptic protein expression

Taken together, the data above suggests that GPER1 is involved in spinogenesis, accompanied by changes in the expression levels of postsynaptic protein PSD95 and also the actin-modulating protein cofilin. Most importantly, the changes mentioned above were all sex-specific and only observed in tissue from females. As I also found that E2 (2 nM) has a sex-specific effect on dendritic spines in SLM in hippocampal slice culture of the Thy1-eGFP mice (Figure 3.6), I wanted to know whether treatment with E2 causes similar changes of expression of PSD95 and G1. As for G1, no changes in expression of ITPKA, SNAP25 and spinophilin were found after treatment of E2 for 24 hours and 48 hours (data not shown).

Similar to the observation of G1 for 24 hours, expression of PSD95 increased significantly in hippocampal slice tissue derived from females, but a nearly significant tendency was also found in males (Figure 3.13A). In addition, in the lysate of cultures that were treated with E2 for 48 hours, PSD95 expression was significantly increased compared to controls both in females and males (Figure 3.13B). Although this may appear contradictory to the G1-data, it should be noted that PSD95-levels did not differ between the sexes also after 48 hours G1-treatment, after which levels were enhanced in both sexes, but the difference did not reach significance (Figure 3.11). Thus, E2 generally replicated the G1-effects.

In contrast, G1-effect on p-cofilin were not replicated after E2-treatment for 48 hours, as the p-/n- cofilin ratio did not change after E2-application.
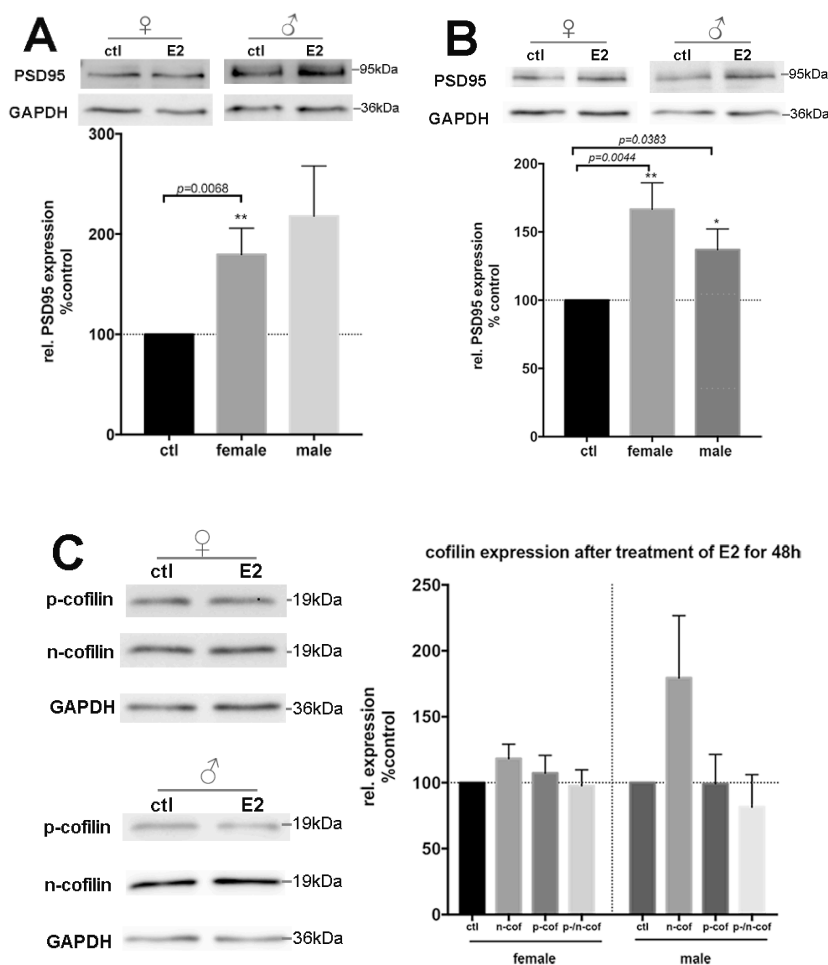
Figure 3.13: Immunoblots and quantification of PSD95 and cofilin expression by western blot analysis after E2-treatment in slice culture. (A) After E2 treatment for 24 hours, significant increase of PSD95 expression was observed in females, and a nearly significant tendency was also observed in males (females: 180±26% of the controls, p=0.0068, n=12 vs. male: 218 ± 50% of the controls, p=0.064, n=11; paired t-test). (B) After E2 treatment for 48 hours, significant increases of PSD95 expression were observed in both sexes (females: 167 ±19% of the controls, *p*=0.0044, n=13 vs. male: 137 ± 15% of the controls, *p*=0.038, n=13; paired t-test). (C) In contrast, no significant differences were found for n-cofilin and p-cofilin expression after E2 treatment for 48 hours in both sexes although n-cofilin expression in males showed a marked trend towards an increase (**n-cof:** females: 118 ± 11% of the controls, *p*=0.19, n=13 vs. male: 179 ± 47% of the controls, *p*=0.3, n=9; **p-cof:** females: 107 ± 13% of the controls, *p*=0.78, n=13 vs. male: 99 ± 22% of the controls, *p*=0.82, n=9; **p-/n-cof:** females: 98 ± 12% of the controls, *p*=0.84, n=9 vs. males: 82 ± 25%, *p* =0.25, n=9; paired t-test). Data are normalized to GAPDH and related to control expression which was set at 100%.

4. Discussion

This study aimed at a better understanding of the functions of the membrane-bound estrogen receptor GPER1 in the hippocampus, and specifically of its functions in the temporoammonic pathway (TA). The major findings of the study are:

1) GPER1 is expressed early postnatally in both the hippocampus and the entorhinal cortex, and its expression increases with maturation. At all developmental stages studied, no sex differences with respect to GPER1 protein expression were evident.

2) In the hippocampus, expression of GPER1 is prominent in CA1 SLM, the termination zone of temporoammonic afferents from the entorhinal cortex.

3) Activation of GPER1 using its agonist G1 resulted in an increased spine density in SLM in entorhino-hippocampal slice cultures from Thy1-eGFP-positive mice. Remarkably, this increase was observed only in slices from female mice, but not in those from male mice.

4) Increased spine density was not accompanied by increased spine synapse density, as the density of spine synapses in SLM was not significantly altered in the slice cultures after G1-treatment in both sexes.

5) Activation of GPER1 using G1 also increased the expression of PSD95 and altered the p-/n-cofilin ratio in the slice cultures sex-specifically (i.e., only in tissue from females).

6) Treatment of the cultures with E2 (2 nM) largely replicated the G1-effects on spine density in SLM and on hippocampal PSD95 expression. However, the p-/n-cofilin ratio was not significantly altered after E2-treatment.

Taken together, these findings indicate that E2 influences spinogenesis in CA1 SLM via GPER1, but may do this sex-specifically. These aspects will be discussed below.

4.1 GPER1 is located at hippocampal sites that may mediate plasticity in the temporoammonic pathway

Previous studies have already revealed the expression of GPER1 in the brain and have reported high levels in the hippocampus of rodents (Brailoiu et al., 2007; Hazell et al., 2009). These studies were later extended by Akama et al. (2013) and Waters et al. (2015), who performed ultrastructural EM-analyses and demonstrated localization of GPER1 both in dendritic spines and in axon terminals. Remarkably, in their studies, GPER1-immunoreactivity is particularly prominent in CA1 SLM and in the stratum lucidum of CA3. Following up on these studies, I initially determined the developmental time course of GPER1 protein expression in the hippocampus of postnatal female mice. The analysis showed the expression was relatively low at P3 but then steadily increased, reaching high level at P17, suggesting that GPER1 expression may increase with maturation (Figure 3.1). This finding is consistent with a previous study (Zhang et al., 2019), which showed the same postnatal pattern. Additionally, the pattern of GPER1 immunoreactivity was determined both in immature and mature female mice. I found that GPER1 localizes strongly to the SLM, the termination zone of the TA, confirming the findings by Waters et al. (2015), and that this pattern is already present in immature (P13) mice (Figure 3.3). A similar expression pattern was also found by Meseke et al. (2018) in P16 rats. Besides, both adolescent and adult mice were used to determine the expression of GPER1 in hippocampus and EC and no sex differences were found (Figure 3.2), in agreement with former findings indicating that no major sexual differences exist in the distribution of GPER1 in rodents (for review, see Alexander et al., 2017). Based on these observations, I expected to find effects after experimental GPER1 manipulation *in vitro* in both sexes.

4.2 Activation of GPER1 modulates spinogenesis in entorhino-hippocampal slice culture of females but not of males

Changes in synaptic plasticity are often accompanied by changes in the number of dendritic spines (Bourne and Harris, 2007). It has long been known that estradiol can regulate dendritic spine density in hippocampus (Mukai et al., 2007; Srivastava et al., 2008; Hasegawa et al., 2015). Previous studies by Smith et al. (2016), revealing altered dendritic spine density in SLM after E2-injection for 24 hours in female rats, indicated that E2 is also a regulator of synaptic plasticity in the TA pathway. The prominent expression of GPER1 in SLM suggests that this plasticity could be mediated by GPER1. In order to test this hypothesis, the GPER1-agonist G1 (Bologa et al., 2006) was applied to entorhino-hippocampal slice cultures from Thy1-eGFP-mice and spine density in SLM was determined.

As shown in Figures 3.4 and 3.5, activation of GPER1 indeed resulted in dendritic spine changes in CA1 SLM in the slice cultures. G1, applied at a concentration of 20 nM for 24 hours or 48 hours, significantly increased the density of non-stubby spines, which are considered spines in process of maturation (Harris et al., 1992). When also taking the more immature stubby spines into account, the total spine number was significantly elevated after 24 hours and showed a marked tendency after 48 hours treatment. In addition, dendritic spine density was also significantly increased after treatment with E2 (2 nM) for 48 hours (Figure 3.6). However, importantly, these effects were seen only in slices from females, but not in those from males, contradictory to what one would expect from the expression studies. This suggests that the underlying mechanisms are not regulated at the GPER1 expression level, but may involve signal transduction via sex-specifically primed signaling cascades (see below; section 4.5).

These data are at some point discrepant to the work from another group, which found increases of spine density in SR after G1 and low-dose E2, but no effects in SLM (Phan et al., 2012, 2015; Gabor et al., 2015). However, as these studies investigated an *in vivo* mouse model after 40 minutes E2 injection, different triggering mechanisms due to the

length of intervention time and the different methodological approaches may be responsible for this discrepancy.

4.3 G1-induced spinogenesis is not accompanied by synaptogenesis in entorhino-hippocampal slice culture

Estradiol has been firmly established to be involved in the regulation of synapse formation in hippocampus not only by our laboratory (Kretz et al., 2004; Bender et al., 2010; Zhou et al., 2010; Vierk et al., 2012) but also by others (Gould et al., 1990; Woolley et al., 1997; Leranth and Shanabrough, 2001). As discussed above, E2 is capable of promoting spinogenesis in CA1 SLM, which is probably mediated by GPER1. Consequently, it was assumed that the increased spinogenesis is accompanied by synaptogenesis, and EM studies were performed to test this hypothesis. However, against expectation, no significant differences were found between G1- and vehicle- treated cultures both after 24 hours and 48 hours (details see section 3.3), indicating G1-induced spinogenesis may not result in synaptogenesis.

Several methodological aspects may explain this discrepancy: first, one needs to consider that the cultures are prepared at an immature stage, at which afferent innervation of the hippocampus is still ongoing and axon density has not yet reached its mature levels (Tamamaki, 1999). In addition, in the organotypic entorhino-hippocampal slice culture model, some of the afferent fibers are cut during preparation and it takes several days for them to regrow (Li et al., 1994). This could have resulted in a shortage of suitable presynaptic partners which could participate in the formation of synapses. Thus, whereas G1- and E2-treatment may have activated spines and "prepared" them for synaptogenesis (Srivastava et al., 2008), synaptogenesis may not have occurred simply due to the lack of afferent partners (Bourne and Harris, 2008). However, it should be noted that the immature state of the cultures also resulted in a relatively poor preservation of tissue, which aggravated the EM analysis.

4.4 Activation of GPER1 regulates synaptic proteins in slice cultures of females but not of males

As referred above, both pre- and post-synaptic elements are required for the stabilization of dendritic spines in hippocampus (for review, see Bourne and Harris, 2008) and changes in spine or synapse densities are usually correlated with changes in the expression levels of synaptic proteins. As GPER1 localization has been described both on pre- and postsynaptic elements (Akama et al., 2013; Waters et al., 2015) and because GPER1 is also expressed in the entorhinal cortex, the site of origin of the TA (Figure 3.2), I determined effects of G1- resp. E2-activation on the expression of selected pre- and postsynaptic marker proteins by Western blotting, using the total lysate of the slice cultures. While no effect was observed for the presynaptic protein SNAP25 and also on some of the studied postsynaptic proteins (ITPKA, spinophilin), the expression of PSD95 was significantly increased both after G1- and E2-application. This is in accordance with a previous study showing that E2 stimulates PSD95 protein translation (Akama and McEwen, 2003). PSD95 is a necessary factor to stabilize dendritic spines as a previous study by Ehrlich et al. (2007) showed that knockdown of PSD95 by RNAi decreases leads to spine loss and prevents functional spine maturation. PSD95 has further been shown to associate with GPER1 in the postsynaptic density (Akama et al., 2013), suggesting that the E2-effect could be mediated via GPER1. These data also validate the chosen experimental model by demonstrating that the organotypic slice cultures respond to E2-treatment in an established manner. Consistently, a significant increase of PSD95-expression was seen after 24 hours only in the female slices, but not in the slices from males, both after treatment with G1 and E2 (Figure 3.11), comparable to the changes of the spine density. After 48 hours, significant changes in the expression of PSD95 were not detectable after G1, but still existed after E2. This may indicate that E2- and G1-signaling are not identical, but that some additional E2-effects interfere (see also Discussion below).

Further, changes in the p-/n-cofilin ratio were observed after G1-treatment. Cofilin regulates actin filament (F-actin) networks, whereby phosphorylated (p)-cofilin promotes the assembly of F-actin, while non-phosphorylated (n)-cofilin promotes the depolymerization of the filaments to G-actin monomers (Fukazawa et al., 2003). As actin is enriched in dendritic spines and is well known to modulate spine/synapse formation (Matus, 2000), the p-/n-cofilin ratio can be considered important for synaptic plasticity. Previous studies suggested that activation of cofilin by dephosphorylation could induce spine remodeling in neurons, resulting in the destabilization and transformation of mature mushroom spine into immature thin spines in hippocampus (Pontrello et al., 2012). In the present study I found that p-/n-cofilin ratio remained unchanged after 24 hours of treatment with G1. But after 48 hours of treatment p-cofilin levels were significantly decreased, resulting in a strongly reduced p-/n-cofilin ratio. These results suggest that GPER1-mediated signaling influences the degree of actin polymerization via modulating the p-/n-cofilin ratio which may increase spine flexibility. This would go along with the G1-induced changes of PSD95, which should promote spine stability (Ehrlich et al., 2007). However, E2-treatment did not replicate the change of the p-/n-cofilin ratio, that was observed after 48 hours G1-treatment, suggesting that other effects, which could be mediated through other E2-receptors, might have interfered with GPER1-mediated signaling. Therefore, more experimentation will be necessary to explain this obviously complex form of G1-induced regulation. However, it should be noted that, in general, G1-effects are replicated after E2-treatment. Thus, in the present study, treatment of the cultures with E2 (2 nM) largely replicated the G1-effects on spine density in SLM and on hippocampal PSD95 expression. Similarly, it was recently found in organotypic entorhino-hippocampal slice cultures that both G1 and E2 caused an increase of the expression of the hyperpolarization-activated ion channel HCN1 in CA1 SLM, and that this effect was prevented if E2 was applied together with the GPER1-antagonist G36 (Meseke et al., 2018). Together, these data indicate that E2-mediated effects in SLM are to a large extent mediated by GPER1.

4.5 Sex differences in GPER1-mediated signaling

It was an unexpected finding that GPER1-induced spinogenesis was only found in slice cultures from female mice, but not in those from male mice. Similarly, G1-mediated changes of synaptic proteins (PSD95, p-cofilin) were only observed in the tissue from female mice, whereas the male tissue did not respond to treatment. This indicates that mechanisms of GPER1-signaling are sex-specific. On the other side, GPER1 expression levels did not differ between male and females, suggesting that the sex difference is not established on the level of receptor expression, but may involve other mechanisms, such as sex-specific intracellular signaling.

Evidence for sex-specific effects of sex hormones in brain is increasing. A study by Vierk et al. (2012) found that the application of letrozole, an inhibitor of the E2-synthesizing enzyme aromatase, causes the loss of spine synapses and strongly reduces long-term potentiation (LTP) specifically in CA1 stratum radiatum of female mice, suggesting that these functions require neuron-derived E2 in females but not in males. In contrast, finasteride, an inhibitor of the enzyme 5α-reductase, which converts testosterone to dihydrotestosterone (DHT), the most potent androgen, reduced spine synapse density and LTP specifically in male hippocampus, suggesting that these functions depend on neuron-derived androgens in males (Brandt et al., 2019). Other studies also revealed sex differences which specifically involve signaling pathways. For example, a study by Tabatadze et al. (2015) showed that E2 acutely suppresses GABAergic inhibition only in female hippocampus through a mechanism that involves ERα, mGluR and endocannaboids. Remarkably, all these sex differences are already established early postnatally, suggesting that they are determined during prenatal development.

Several examples for a sex-specific determination are described in the literature. For example, the exposure of neonatal hippocampal and striatal neurons to E2 or testosterone alters their responsiveness to estradiol throughout life, presumably due to sex-specific priming of estrogen receptor signaling (Meitzen et al., 2012, 2013). It can therefore be

assumed that sex hormones promote a sex-specific organization in neurons during certain developmental phases (McCarthy and Arnold, 2011). This organization may be associated with a developmental surge of testosterone specifically in males which occurs perinatally in rodents (Chung and Auger, 2013). The sex-specific effects of GPER1-activation observed in this study could be a consequence of the same sex-specific priming. However, additional investigations need to be performed to confirm the hypothesis. It would further be interesting to determine whether these differences are only observed during the developmental period or are preserved into adulthood, in which they could underly certain sex-specific behavior effects observed in GPER1 KO mice (Kastenberger and Schwarzer, 2014, see also Disscussion below).

4.6 GPER1 in the central nervous system

Previous studies have demonstrated effects of estrogen on synaptic plasticity and other beneficial effects in the human brain (shown in Section 1.2 and 1.3). These effects have mostly been attributed to the functions of the classical estrogen receptors ERα and ERβ. However, as a membrane-bound receptor for estrogen, GPER1 is also good candidate to regulate memory functions and cognition, and to provide neuroprotection (for review, see Alexander et al., 2017). Hammond et al. (2009) were the first to show that G1 can enhance spatial learning in ovariectomized rats in the delayed-matching-to-position (DMP) T-maze task, and they provided further support that inhibition of GPER1 with G15 could impair spatial learning. Similarly, rapid enhancing effects of G1 on social recognition, object recognition and object placement learning were observed after subcutaneous administration with G1 in ovariectomized CD1 mice (Gabor et al., 2015). Further, short-term treatment of ovariectomized rats with G1 enhanced spatial recognition memory in parallel with a low dose of estradiol (Hawley et al., 2014).

GPER1 also appears to modify social behaviors, for example through regulating the state of anxiety (for review, see Hadjimarkou and Vasudevan, 2018). Kastenberger et al. (2012) found that stimulation of GPER1 with G1 induced anxiogenic effects in both male and

ovariectomized female mice. They confirmed their results with GPER1 knock out mice, in which they found sex differences, as increased exploration and decreased anxiety were observed in male GPER1 KO mice, while the female GPER1-KO mice displayed a less pronounced phenotype in these tests (Kastenberger and Schwarzer, 2014). In support, Hart et al (2014) confirmed the potential sex-specific function of GPER1 on the state of anxiety as they reported an anxiolytic effect of GPER1 activation in male mice.

With respect to neuroprotection, Tang et al. (2014) reported that G1 exerts neuroprotection against global cerebral ischemia by activating Akt and ERK (the pro-survival kinases) rapidly. Lebesgue et al. (2010) reported G1-induced neuroprotective effects during ischemia in hippocampal neurons of middle-aged female rats. In a Parkinson's disease mouse model, G1 was identified to attenuate the decrease of dopamine in myenteric neurons and enteric macrophage infiltration while G15 could block such anti-inflammatory and neuroprotective effects of G1 (Côté et al., 2015).

4.7 GPER1 in other organs

In addition to the CNS, GPER1 is widely expressed in other tissues, including heart, intestine, ovary, pancreatic islets, adipose tissue, inflammatory cells (Shi et al., 2013), and appears to be implicated in diverse physiological processes including immune, cardiovascular and metabolic functions (for review, see Sharma et al., 2018).

Further, GPER1 plays an important role in breast and gynecological cancers (for review, see Barton et al., 2018). For example, GPER1 is expressed in 50- 60% of breast cancer tissues and is prevalent in triple-negative breast cancer (Hsu et al., 2019). Ample evidence has demonstrated its relationship with tumor progression and poor survival, but GPER1 showed an inhibitory effect when ERα is present (Liu et al., 2014). Besides, expression of GPER1 in tumors is associated with resistance of tamoxifen, a pharmacological agent mixed with ER antagonists (for review, see Filardo, 2018). The role of GPER1 in ovarian cancer is still controversial. Smith et al. (2009) associated GPER1 expression with poor

survival in ovarian patients while Ignatov et al. (2013) suggested GPER1 may be a tumor suppressor as G1 inhibited the proliferation of ovarian cancer cells. Taken together, GPER1 can be considered a biological target for innovative therapeutic strategies in breast and gynecological cancers. However, as the results of this study suggest, effects on synaptic plasticity in brain need to be considered.

4.8 Limitations of the study

In summary, I found that activation of GPER1 using its agonist G1 modifies spine density in SLM, increases expression of PSD95 and alteres the p-/n-cofilin ratio in entorhino-hippocampal slice cultures. Most importantly, these effects are sex-dependent and observed only in slice cultures from females, but not in those from males. Treatment of the cultures with E2 (2 nM) largely replicated the G1-effects on spine density in SLM and on hippocampal PSD95 expression. These results are encouraging with respect to achieving a better understanding of the functions of GPER1 in hippocampus and their differential regulation in the tissue from males and females.

However, it needs to be pointed out that all experiments presented were performed with immature tissue, which limits our conclusions only to the developmental time period and to the specific conditions which are offered by the organotypic slice culture model. This model has many advantages, as it offers an easy accessibility for experimental manipulation over a reasonable time period (Stoppini et al., 1991). However, it is still an artificial model, because the slice cultures have lost most of their natural neuronal connections and are kept alive in an artificial environment. Similarly, the developmental age may be important for interpreting the data. For example, there exist differences in the types of dendritic spines and synapses between adult and immature animals. Experiments performed with immature rats demonstrated that before P15, synapses primarily occurred on dendritic shafts and stubby spines but in young adult rats, most synapses are likely to be formed on longer thin spines (Fiala et al., 1998). Age-dependent differences of hormonal exposure should also be taken into consideration. For example, GPER1 effects could differ in post-pubertal

animals, when testosterone levels have further risen in the males, and estrous cycle has begun in the females. Therefore, experiments *in vivo* will be necessary to support and strengthen the presented findings. As GPER1-deficient are available (Wang et al., 2008), they provide an attractive tool for future studies.

5. Summary

The CA1 region of the hippocampus receives input from the entorhinal cortex through two pathways, indirectly via the classic "trisynaptic" path and directly through the temporoammonic pathway (TA). The contribution of 17β-estradiol (E2) to neuronal plasticity in hippocampal CA1 has been widely investigated, but studies have focused on CA1 stratum radiatum, the termination zone of the "trisynaptic" path, whereas the functions of E2 in CA1 stratum lacunosum (SLM), the termination zone of the TA, are poorly understood. Prompted by observations of a strong expression of the membrane-bound estrogen receptor GPER1 in SLM, this study aimed at an understanding of E2-mediated functions via GPER1 in SLM. Using GPER1-agonist G1 and organotypic entorhino-hippocampal slice cultures from Thy1-eGFP-mice for *in vitro* experimentation, effects of GPER1 activation on the densities of spines and spine synapses were determined in SLM. In addition, effects of G1 on the expression of synaptic proteins were determined by Western Blots in the culture lysate. Effects of E2-treatment (2 nM) were measured for comparison. The experiments revealed increased spine densities and altered expression levels of synaptic proteins (enhanced PSD95, reduced p-/n-cofilin ratio) in the slice cultures after G1-treatment. Remarkably, these effects were sex-dependent and observed only in cultures from female mice, and not in those from male mice. E2-treatment largely replicated the findings after G1, indicating that the observed effects can be attributed to estrogen. However, some discrepancies after E2-treatment also suggest that E2-signaling pathways in SLM do not only involve GPER1. In addition, spinogenesis was not accompanied by synaptogenesis in the G1-treated slice cultures, which, however, could be explained by the immature state of the cultures and other methodological aspects. Taken together, these findings support potential functions of GPER1 in estrogen-mediated neuronal plasticity and could be relevant for the understanding of sex differences in memory-related cognitive functions. Follow-up studies using GPER1-deficient mouse lines may further throw light on the functions of this receptor in SLM.

Zusammenfassung

Die CA1-Region des Hippocampus erhält Eingänge vom entorhinalen Kortex über zwei Wege, indirekt über den klassischen „trisynaptischen Pfad" und direkt über den „temporoammonischen Pfad" (TA). Untersuchungen zur Rolle von 17β-Östradiol (E2) bei der Regulation neuronaler Plastizität in der CA1-Region konzentrierten sich bislang auf das Stratum radiatum, die Terminationszone des trisynaptischen Pfades. Relativ wenig untersucht, sind Funktionen von E2 im Stratum lacunosum-moleculare (SLM), der Terminationszone des TA. Veranlasst durch den Befund einer markanten Expression des membranständigen Östrogenrezeptors GPER1 im SLM, untersuchte diese Studie mögliche GPER1-vermittelte Funktionen im SLM. Dabei wurden der GPER1-Agonist G1 und organotypische, entorhino-hippocampale Gewebekulturen von Thy1-eGFP-positiven Mäusen für Experimente *in vitro* genutzt. Untersucht wurden die Auswirkungen einer G1-vermittelten GPER1-Aktivierung auf die Dichte von Dornfortsätzen (*Spines*) und von *Spine*synapsen im SLM. Weiterhin wurden im Lysat der Kulturen die Auswirkungen einer G1-Behandlung auf die Expression synaptischer Proteine mittels Western Blots bestimmt. Begleitend wurden dieselben Parameter auch nach E2-Stimulierung (2 nM) untersucht. Die Untersuchungen erbrachten den Befund, dass die *Spine*dichte im SLM nach G1-Gabe signifikant erhöht war. Zusätzlich wurde durch G1 auch die Expression von PSD95 erhöht und das Verhältnis von p- zu n-Cofilin reduziert. Bemerkenswerterweise waren diese Effekte jedoch nur in Kulturen von weiblichen Mäusen, nicht aber in denen von männlichen, zu beobachten. E2-Gabe reproduzierte die G1-Befunde weitgehend, was auf E2 als Effektor hindeutet. Einige E2-Wirkungen waren jedoch diskrepant zu den G1-Effekten, was möglicherweise durch zusätzliche Östrogenrezeptor-Wirkungen im SLM zu erklären ist. Außerdem war die *Spine*zunahme nach G1-Gabe nicht von einer Zunahme von *Spine*synapsen begleitet, was jedoch durch das frühe Entwicklungsstadium der Gewebekulturen und methodische Aspekte erklärbar ist. Zusammengenommen unterstützen diese Befunde die Annahme einer Bedeutung von GPER1 bei der E2-

vermittelten neuronalen Plastizität im Hippocampus und sie könnten für das Verständnis von Geschlechtsunterschieden in gedächtnisbezogenen kognitiven Funktionen relevant sein. Zukünftige Untersuchungen an GPER1-defizienten Mäusen könnten weitere Erkenntnisse über die Funktion dieses Rezeptors erbringen.

6. References

Akama KT, McEwen BS (2003) Estrogen stimulates postsynaptic density-95 rapid protein synthesis via the Akt/protein kinase B pathway. J Neurosci 23:2333–2339.

Akama KT, Thompson LI, Milner TA, McEwen BS (2013) Post-synaptic density-95 (PSD-95) binding capacity of G-protein-coupled receptor 30 (GPR30), an estrogen receptor that can be identified in hippocampal dendritic spines. J Biol Chem 288:6438–6450.

Alexander A, Irving AJ, Harvey J (2017) Emerging roles for the novel estrogen-sensing receptor GPER1 in the CNS. Neuropharmacology 113:652–660.

Almey A, Filardo EJ, Milner TA, Brake WG (2012) Estrogen Receptors Are Found in Glia and at Extranuclear Neuronal Sites in the Dorsal Striatum of Female Rats: Evidence for Cholinergic But Not Dopaminergic Colocalization. Endocrinology 153:5373–5383.

Almey A, Milner TA, Brake WG (2015) Estrogen receptors in the central nervous system and their implication for dopamine-dependent cognition in females. Horm Behav 74:125–138.

Amaral DG, Scharfman HE, Lavenex P (2007) The dentate gyrus: fundamental neuroanatomical organization (dentate gyrus for dummies). Prog Brain Res 163:3–22.

Antonucci F, Corradini I, Fossati G, Tomasoni R, Menna E, Matteoli M (2016) SNAP-25, a Known presynaptic protein with emerging postsynaptic functions. Front Synaptic Neurosci 8:1–9.

Balthazart J, Ball GF (2006) Is brain estradiol a hormone or a neurotransmitter? Trends Neurosci 29:241–249.

Barton M, Filardo EJ, Lolait SJ, Thomas P, Maggiolini M, Prossnitz ER (2018) Twenty years of the G protein-coupled estrogen receptor GPER: Historical and personal perspectives. J Steroid Biochem Mol Biol 176:4–15.

Baulieu EE, Robel P (1990) Neurosteroids: a new brain function? J Steroid Biochem Mol Biol 37:395–403.

Bayer J, Rune G, Schultz H, Tobia MJ, Mebes I, Katzler O, Sommer T (2015) The effect of estrogen synthesis inhibition on hippocampal memory. Psychoneuroendocrinology 56:213–225.

Bender RA, Baram TZ (2008) Hyperpolarization activated cyclic-nucleotide gated (HCN) channels in developing neuronal networks. Prog Neurobiol 86:129–140.

Bender RA, Zhou L, Vierk R, Brandt N, Keller A, Gee CE, Schäfer MKE, Rune GM (2017) Sex-Dependent Regulation of Aromatase-Mediated Synaptic Plasticity in the Basolateral Amygdala. J Neurosci 37:1532–1545.

Bender RA, Zhou L, Wilkars W, Fester L, Lanowski J-S, Paysen D, Konig A, Rune GM (2010) Roles of 17ss-estradiol involve regulation of reelin expression and synaptogenesis in the dentate gyrus. Cereb Cortex 20:2985–2995.

Bologa CG, Revankar CM, Young SM, Edwards BS, Arterburn JB, Kiselyov AS, Parker MA, Tkachenko SE, Savchuck NP, Sklar LA, Oprea TI, Prossnitz ER (2006) Virtual and biomolecular screening converge on a selective agonist for GPR30. Nat Chem Biol 2:207–212.

Bourne J, Harris KM (2007) Do thin spines learn to be mushroom spines that remember? Curr Opin Neurobiol 17:381–386.

Bourne JN, Harris KM (2008) Balancing structure and function at hippocampal dendritic spines. Annu Rev Neurosci 31:47–67.

Bradford MM (1976) A rapid and sensitive method for the quantitation of microgram quantities of protein utilizing the principle of protein-dye binding. Anal Biochem 72:248–254.

Brailoiu E, Dun SL, Brailoiu GC, Mizuo K, Sklar LA, Oprea TI, Prossnitz ER, Dun NJ (2007) Distribution and characterization of estrogen receptor G protein-coupled receptor 30 in the rat central nervous system. J Endocrinol 193:311–321.

Brandt N, Vierk R, Fester L, Anstötz M, Zhou L, Heilmann LF, Kind S, Steffen P, Rune GM (2019) Sex-specific Difference of Hippocampal Synaptic Plasticity in Response to Sex Neurosteroids. Cereb Cortex.

Broadhead MJ, Horrocks MH, Zhu F, Muresan L, Benavides-Piccione R, DeFelipe J, Fricker D, Kopanitsa M V., Duncan RR, Klenerman D, Komiyama NH, Lee SF, Grant SGN (2016) PSD95 nanoclusters are postsynaptic building blocks in hippocampus circuits. Sci Rep 6:1–14.

Brun VH, Otnass MK, Molden S, Steffenach H-A, Witter MP, Moser M-B, Moser EI (2002) Place cells and place recognition maintained by direct entorhinal-hippocampal circuitry. Science 296:2243–2246.

Carmeci C, Thompson DA, Ring HZ, Francke U, Weigel RJ (1997) Identification of a Gene (GPR30) with Homology to the G-Protein-Coupled Receptor Superfamily Associated with Estrogen Receptor Expression in Breast Cancer. Genomics 45:607–617.

Chen X, Vinade L, Leapman RD, Petersen JD, Nakagawa T, Phillips TM, Sheng M, Reese TS (2005) Mass of the postsynaptic density and enumeration of three key molecules. Proc Natl Acad Sci U S A 102:11551–11556.

Cho KO, Hunt CA, Kennedy MB (1992) The rat brain postsynaptic density fraction contains a homolog of the Drosophila discs-large tumor suppressor protein. Neuron 9:929–942.

Chung WCJ, Auger AP (2013) Gender differences in neurodevelopment and epigenetics. Pflugers Arch 465:573–584.

Côté M, Bourque M, Poirier AA, Aubé B, Morissette M, Di Paolo T, Soulet D (2015) GPER1-mediated immunomodulation and neuroprotection in the myenteric plexus of a mouse model of Parkinson's disease. Neurobiol Dis 82:99–113.

Dennis MK, Burai R, Ramesh C, Petrie WK, Alcon SN, Nayak TK, Bologa CG, Leitao A, Brailoiu E, Deliu E, Dun NJ, Sklar LA, Hathaway HJ, Arterburn JB, Oprea TI, Prossnitz ER (2009) In vivo effects of a GPR30 antagonist. Nat Chem Biol 5:421–427.

Dennis MK, Field AS, Burai R, Ramesh C, Petrie WK, Bologa CG, Oprea TI, Yamaguchi Y, Hayashi S-I, Sklar LA, Hathaway HJ, Arterburn JB, Prossnitz ER (2011) Identification of a GPER/GPR30 antagonist with improved estrogen receptor counterselectivity. J Steroid Biochem Mol Biol 127:358–366.

Ehrlich I, Klein M, Rumpel S, Malinow R (2007) PSD-95 is required for activity-driven synapse stabilization. Proc Natl Acad Sci U S A 104:4176–4181.

Feng G, Mellor RH, Bernstein M, Keller-Peck C, Nguyen QT, Wallace M, Nerbonne JM, Lichtman JW, Sanes JR (2000a) Imaging neuronal subsets in transgenic mice expressing multiple spectral variants of GFP. Neuron 28:41–51.

Feng J, Yan Z, Ferreira A, Tomizawa K, Liauw JA, Zhuo M, Allen PB, Ouimet CC, Greengard P (2000b) Spinophilin regulates the formation and function of dendritic spines. Proc Natl Acad Sci U S A 97:9287–9292.

Fester L, Rune GM (2015) Sexual neurosteroids and synaptic plasticity in the hippocampus. Brain Res 1621:162–169.

Fester L, Zhou L, Butow A, Huber C, von Lossow R, Prange-Kiel J, Jarry H, Rune GM (2009) Cholesterol-promoted synaptogenesis requires the conversion of cholesterol to estradiol in the hippocampus. Hippocampus 19:692–705.

Fester L, Zhou L, Ossig C, Labitzke J, Blaute C, Bader M, Vollmer G, Jarry H, Rune GM (2017) Synaptopodin is regulated by aromatase activity. J Neurochem 140:126–139.

Fiala JC, Feinberg M, Popov V, Harris KM (1998) Synaptogenesis via dendritic filopodia in developing hippocampal area CA1. J Neurosci 18:8900–8911.

Filardo EJ (2018) A role for G-protein coupled estrogen receptor (GPER) in estrogen-induced carcinogenesis: Dysregulated glandular homeostasis, survival and metastasis. J Steroid Biochem Mol Biol 176:38–48.

Foy MR, Xu J, Xie X, Brinton RD, Thompson RF, Berger TW (1999) 17beta-estradiol enhances NMDA receptor-mediated EPSPs and long-term potentiation. J Neurophysiol 81:925–929.

Frick KM, Kim J, Tuscher JJ, Fortress AM (2015) Sex steroid hormones matter for learning and memory: Estrogenic regulation of hippocampal function in male and female rodents. Learn Mem 22:472–493.

Fukazawa Y, Saitoh Y, Ozawa F, Ohta Y, Mizuno K, Inokuchi K (2003) Hippocampal LTP is accompanied by enhanced F-actin content within the dendritic spine that is essential for late LTP maintenance in vivo. Neuron 38:447–460.

Funakoshi T, Yanai A, Shinoda K, Kawano MM, Mizukami Y (2006) G protein-coupled receptor 30 is an estrogen receptor in the plasma membrane. Biochem Biophys Res Commun 346:904–910.

Gabor C, Lymer J, Phan A, Choleris E (2015) Rapid effects of the G-protein coupled oestrogen receptor (GPER) on learning and dorsal hippocampus dendritic spines in female mice. Physiol Behav 149:53–60.

Gould E, Woolley CS, Frankfurt M, McEwen BS (1990) Gonadal steroids regulate dendritic spine density in hippocampal pyramidal cells in adulthood. J Neurosci 10:1286–1291.

Hadjimarkou MM, Vasudevan N (2018) GPER1/GPR30 in the brain: Crosstalk with classical estrogen receptors and implications for behavior. J Steroid Biochem Mol Biol 176:57–64.

Hammond R, Mauk R, Ninaci D, Nelson D, Gibbs RB (2009) Chronic treatment with estrogen receptor agonists restores acquisition of a spatial learning task in young ovariectomized rats. Horm Behav 56:309–314.

Hammond R, Nelson D, Kline E, Gibbs RB (2012) Chronic treatment with a GPR30 antagonist impairs acquisition of a spatial learning task in young female rats. Horm Behav 62:367–374.

Harris KM, Jensen FE, Tsao B (1992) Three-Dimensional Structure of Dendritic Spines and Synapses in Rat Hippocampus (CAI) at Postnatal Day 15 and Adult Ages: Implications for the Maturation of Synaptic Physiology and Long-term Potentiation. J Neurosci 12:2685–2705.

Hasegawa Y, Hojo Y, Kojima H, Ikeda M, Hotta K, Sato R, Ooishi Y, Yoshiya M, Chung BC, Yamazaki T, Kawato S (2015) Estradiol rapidly modulates synaptic plasticity of hippocampal neurons: Involvement of kinase networks. Brain Res 1621:147–161.

Hawley WR, Grissom EM, Moody NM, Dohanich GP, Vasudevan N (2014) Activation of G-protein-coupled receptor 30 is sufficient to enhance spatial recognition memory in ovariectomized rats. Behav Brain Res 262:68–73.

Hazell GGJ, Yao ST, Roper JA, Prossnitz ER, O'Carroll A-M, Lolait SJ (2009) Localisation of GPR30, a novel G protein-coupled oestrogen receptor, suggests multiple functions in rodent brain and peripheral tissues. J Endocrinol 202:223–236.

Hojo Y, Hattori T -a., Enami T, Furukawa A, Suzuki K, Ishii H -t., Mukai H, Morrison JH, Janssen WGM, Kominami S, Harada N, Kimoto T, Kawato S (2004) Adult male rat hippocampus synthesizes estradiol from pregnenolone by cytochromes P45017 and P450 aromatase localized in neurons. Proc Natl Acad Sci 101:865–870.

Hojo Y, Murakami G, Mukai H, Higo S, Hatanaka Y, Ogiue-Ikeda M, Ishii H, Kimoto T, Kawato S (2008) Estrogen synthesis in the brain—Role in synaptic plasticity and memory. Mol Cell Endocrinol 290:31–43.

Hsu L-H, Chu N-M, Lin Y-F, Kao S-H (2019) G-Protein Coupled Estrogen Receptor in Breast Cancer. Int J Mol Sci 20:306.

Ignatov T, Modl S, Thulig M, Weißenborn C, Treeck O, Ortmann O, Zenclussen A, Costa S, Kalinski T, Ignatov A (2013) GPER-1 acts as a tumor suppressor in ovarian cancer. J Ovarian Res 6:51.

Janicki SC, Schupf N (2010) Hormonal influences on cognition and risk for Alzheimer's disease. Curr Neurol Neurosci Rep 10:359–366.

Jelks KB, Wylie R, Floyd CL, McAllister AK, Wise P (2007) Estradiol targets synaptic proteins to induce glutamatergic synapse formation in cultured hippocampal neurons: critical role of estrogen receptor-alpha. J Neurosci 27:6903–6913.

Kastenberger I, Lutsch C, Schwarzer C (2012) Activation of the G-protein-coupled receptor GPR30 induces anxiogenic effects in mice, similar to oestradiol. Psychopharmacology (Berl) 221:527–535.

Kastenberger I, Schwarzer C (2014) GPER1 (GPR30) knockout mice display reduced anxiety and altered stress response in a sex and paradigm dependent manner. Horm Behav 66:628–636.

Köster JD, Leggewie B, Blechner C, Brandt N, Fester L, Rune G, Schweizer M, Kindler S, Windhorst S (2016) Inositol-1,4,5-trisphosphate-3-kinase-A controls morphology of hippocampal dendritic spines. Cell Signal 28:83–90.

Kramar EA, Chen LY, Brandon NJ, Rex CS, Liu F, Gall CM, Lynch G (2009) Cytoskeletal changes underlie estrogen's acute effects on synaptic transmission and plasticity. J Neurosci 29:12982–12993.

Kretz O, Fester L, Wehrenberg U, Zhou L, Braukmann S, Zhao S, Prange-Kiel J, Naumann T, Jarry H, Frotscher M, Rune GM (2004) Hippocampal Synapses Depend on Hippocampal Estrogen Synthesis. J Neurosci 24:5913–5921.

Laemmli UK (1970) Cleavage of structural proteins during the assembly of the head of bacteriophage T4. Nature 227:680–685.

Lebesgue D, Traub M, De Butte-Smith M, Chen C, Zukin RS, Kelly MJ, Etgen AM (2010) Acute administration of non-classical estrogen receptor agonists attenuates ischemia-induced hippocampal neuron loss in middle-aged female rats. PLoS One 5:e8642.

Leranth C, Shanabrough M (2001) Supramammillary area mediates subcortical estrogenic action on hippocampal synaptic plasticity. Exp Neurol 167:445–450.

Li D, Field PM, Yoshioka N, Raisman G (1994) Axons regenerate with correct specificity in horizontal slice culture of the postnatal rat entorhino-hippocampal system. Eur J Neurosci 6:1026–1037.

Li Y, Xu J, Liu Y, Zhu J, Liu N, Zeng W, Huang N, Rasch MJ, Jiang H, Gu X, Li X, Luo M, Li C, Teng J, Chen J, Zeng S, Lin L, Zhang X (2017) A distinct entorhinal cortex to hippocampal CA1 direct circuit for olfactory associative learning. Nat Neurosci 20:559–570.

Liu H, Yan Y, Wen H, Jiang X, Cao X, Zhang G, Liu G (2014) A novel estrogen receptor GPER mediates proliferation induced by 17beta-estradiol and selective GPER agonist G-1 in estrogen receptor alpha (ERalpha)-negative ovarian cancer cells. Cell Biol Int 38:631–638.

Maccaferri G (2011) Modulation of hippocampal stratum lacunosum-moleculare microcircuits. J Physiol 589:1885–1891.

Mailleux P, Takazawa K, Erneux C, Vanderhaeghen JJ (1993) Distribution of the neurons containing inositol 1,4,5-trisphosphate 3-kinase and its messenger RNA in the developing rat brain. J Comp Neurol 327:618–629.

Manns JR, Zilli EA, Ong KC, Hasselmo ME, Eichenbaum H (2007) Hippocampal CA1 spiking during encoding and retrieval: relation to theta phase. Neurobiol Learn Mem 87:9–20.

Martin J (2003) Neuroanatomy: text and Atlas. McGraw-Hill companies.

Matus A (2000) Actin-based plasticity in dendritic spines. Science 290:754–758.

McCarthy MM, Arnold AP (2011) Reframing sexual differentiation of the brain. Nat Neurosci 14:677–683.

McEwen BS, Alves SE (1999) Estrogen actions in the central nervous system. Endocr Rev 20:279–307.

McGregor G, Harvey J (2019) Leptin Regulation of Synaptic Function at Hippocampal TA-CA1 and SC-CA1 Synapses: Implications for Health and Disease. Neurochem Res 44:650–660.

Meitzen J, Grove DD, Mermelstein PG (2012) The organizational and aromatization hypotheses apply to rapid, nonclassical hormone action: neonatal masculinization eliminates rapid estradiol action in female hippocampal neurons. Endocrinology 153:4616–4621.

Meitzen J, Perry AN, Westenbroek C, Hedges VL, Becker JB, Mermelstein PG (2013) Enhanced striatal beta1-adrenergic receptor expression following hormone loss in adulthood is programmed by both early sexual differentiation and puberty: a study of humans and rats. Endocrinology 154:1820–1831.

Meseke M, Neumuller F, Brunne B, Li X, Anstotz M, Pohlkamp T, Rogalla MM, Herz J, Rune GM, Bender RA (2018) Distal Dendritic Enrichment of HCN1 Channels in Hippocampal CA1 Is Promoted by Estrogen, but Does Not Require Reelin. eNeuro 5.

Mukai H et al. (2007) Rapid modulation of long-term depression and spinogenesis via synaptic estrogen receptors in hippocampal principal neurons. J Neurochem 100:950–967.

Neves G, Cooke SF, Bliss TVP (2008) Synaptic plasticity, memory and the hippocampus: A neural network approach to causality. Nat Rev Neurosci 9:65–75.

Paul SM, Purdy RH (1992) Neuroactive steroids. FASEB J Off Publ Fed Am Soc Exp Biol 6:2311–2322.

Phan A, Gabor CS, Favaro KJ, Kaschack S, Armstrong JN, MacLusky NJ, Choleris E (2012) Low doses of 17beta-estradiol rapidly improve learning and increase hippocampal dendritic spines. Neuropsychopharmacology 37:2299–2309.

Phan A, Suschkov S, Molinaro L, Reynolds K, Lymer JM, Bailey CDC, Kow L-M, MacLusky NJ, Pfaff DW, Choleris E (2015) Rapid increases in immature synapses parallel estrogen-induced hippocampal learning enhancements. Proc Natl Acad Sci U S A 112:16018–16023.

Pontrello CG, Sun M-Y, Lin A, Fiacco TA, DeFea KA, Ethell IM (2012) Cofilin under control of beta-arrestin-2 in NMDA-dependent dendritic spine plasticity, long-term depression (LTD), and learning. Proc Natl Acad Sci U S A 109:E442-51.

Prange-Kiel J, Dudzinski DA, Prols F, Glatzel M, Matschke J, Rune GM (2016) Aromatase Expression in the Hippocampus of AD Patients and 5xFAD Mice. Neural Plast 2016:9802086.

Prange-Kiel J, Schmutterer T, Fester L, Zhou L, Imholz P, Brandt N, Vierk R, Jarry H, Rune GM (2013) Endocrine regulation of estrogen synthesis in the hippocampus? Prog Histochem Cytochem 48:49–64.

Prange-Kiel J, Wehrenberg U, Jarry H, Rune GM (2003) Para/autocrine regulation of estrogen receptors in hippocampal neurons. Hippocampus 13:226–234.

Prossnitz ER, Arterburn JB, Smith HO, Oprea TI, Sklar LA, Hathaway HJ (2008) Estrogen signaling through the transmembrane G protein-coupled receptor GPR30. Annu Rev Physiol 70:165–190.

Prossnitz ER, Barton M (2011) The G-protein-coupled estrogen receptor GPER in health and disease. Nat Rev Endocrinol 7:715–726.

Remondes M, Schuman EM (2004) Role for a cortical input to hippocampal area CA1 in the consolidation of a long-term memory. Nature 431:699–703.

Revankar CM, Cimino DF, Sklar LA, Arterburn JB, Prossnitz ER (2005) A transmembrane intracellular estrogen receptor mediates rapid cell signaling. Science 307:1625–1630.

Satoh A, Nakanishi H, Obaishi H, Wada M, Takahashi K, Satoh K, Hirao K, Nishioka H, Hata Y, Mizoguchi A, Takai Y (1998) Neurabin-II/spinophilin. An actin filament-binding protein with one pdz domain localized at cadherin-based cell-cell adhesion sites. J Biol Chem 273:3470–3475.

Sharma G, Mauvais-Jarvis F, Prossnitz ER (2018) Roles of G protein-coupled estrogen receptor GPER in metabolic regulation. J Steroid Biochem Mol Biol 176:31–37.

Shi H, Kumar SPDS, Liu X (2013) G protein-coupled estrogen receptor in energy homeostasis and obesity pathogenesis. Prog Mol Biol Transl Sci 114:193–250.

Smith CC, Smith LA, Bredemann TM, McMahon LL (2016) 17β estradiol recruits GluN2B-containing NMDARs and ERK during induction of long-term potentiation at temporoammonic-CA1 synapses. Hippocampus 26:110–117.

Smith HO, Arias-Pulido H, Kuo DY, Howard T, Qualls CR, Lee S-J, Verschraegen CF, Hathaway HJ, Joste NE, Prossnitz ER (2009) GPR30 predicts poor survival for ovarian cancer. Gynecol Oncol 114:465–471.

Srivastava DP, Evans PD (2013) G-protein oestrogen receptor 1: trials and tribulations of a membrane oestrogen receptor. J Neuroendocrinol 25:1219–1230.

Srivastava DP, Waters EM, Mermelstein PG, Kramar EA, Shors TJ, Liu F (2011) Rapid Estrogen Signaling in the Brain: Implications for the Fine-Tuning of Neuronal Circuitry. J Neurosci 31:16056–16063.

Srivastava DP, Woolfrey KM, Jones KA, Shum CY, Lash LL, Swanson GT, Penzes P (2008) Rapid enhancement of two-step wiring plasticity by estrogen and NMDA receptor activity. Proc Natl Acad Sci 105:14650–14655.

Standring S (2015) Gray's Anatomy The Anatomical basis of calinical practice, 41st ed. Philadelphia: Elsevier.

Sterio DC (1984) The unbiased estimation of number and sizes of arbitrary particles using the disector. J Microsc 134:127–136.

Stoppini L, Buchs PA, Muller D (1991) A simple method for organotypic cultures of nervous tissue. J Neurosci Methods 37:173–182.

Suh J, Rivest AJ, Nakashiba T, Tominaga T, Tonegawa S (2011) Entorhinal cortex layer III input to the hippocampus is crucial for temporal association memory. Science 334:1415–1420.

Tabatadze N, Huang G, May RM, Jain A, Woolley CS (2015) Sex Differences in Molecular Signaling at Inhibitory Synapses in the Hippocampus. J Neurosci 35:11252–11265.

Tamamaki N (1999) Development of afferent fiber lamination in the infrapyramidal blade of the rat dentate gyrus. J Comp Neurol 411:257–266.

Tang H, Zhang Q, Yang L, Dong Y, Khan M, Yang F, Brann DW, Wang R (2014) GPR30 Mediates Estrogen Rapid Signaling and Neuroprotection. Mol Cell Endocrinol 387:52–58.

Thomas P, Pang Y, Filardo EJ, Dong J (2005) Identity of an estrogen membrane receptor coupled to a G protein in human breast cancer cells. Endocrinology 146:624–632.

Vasudevan N, Pfaff DW (2008) Non-genomic actions of estrogens and their interaction with genomic actions in the brain. Front Neuroendocrinol 29:238–257.

Vierk R, Glassmeier G, Zhou L, Brandt N, Fester L, Dudzinski D, Wilkars W, Bender RA, Lewerenz M, Gloger S, Graser L, Schwarz J, Rune GM (2012) Aromatase Inhibition Abolishes LTP Generation in Female But Not in Male Mice. J Neurosci 32:8116–8126.

Wang C, Dehghani B, Magrisso IJ, Rick EA, Bonhomme E, Cody DB, Elenich LA, Subramanian S, Murphy SJ, Kelly MJ, Rosenbaum JS, Vandenbark AA, Offner H (2008) GPR30 contributes to estrogen-induced thymic atrophy. Mol Endocrinol 22:636–648.

Waters EM, Thompson LI, Patel P, Gonzales AD, Ye H, Filardo EJ, Clegg DJ, Gorecka J, Akama KT, McEwen BS, Milner TA (2015) G-Protein-Coupled Estrogen Receptor 1 Is Anatomically Positioned to Modulate Synaptic Plasticity in the Mouse Hippocampus. J Neurosci 35:2384–2397.

Waxman SG (2013) Clinical Neuroanatomy, 27th ed. New York: McGraw-Hill Publishing.

Witter MP, Doan TP, Jacobsen B, Nilssen ES, Ohara S (2017) Architecture of the Entorhinal Cortex A Review of Entorhinal Anatomy in Rodents with Some Comparative Notes. Front Syst Neurosci 11:46.

Woolley CS (2007) Acute Effects of Estrogen on Neuronal Physiology. Annu Rev Pharmacol Toxicol 47:657–680.

Woolley CS, McEwen BS (1992) Estradiol mediates fluctuation in hippocampal synapse density during the estrous cycle in the adult rat. J Neurosci 12:2549–2554.

Woolley CS, Weiland NG, McEwen BS, Schwartzkroin PA (1997) Estradiol Increases the Sensitivity of Hippocampal CA1 Pyramidal Cells to NMDA Receptor-Mediated Synaptic Input: Correlation with Dendritic Spine Density. J Neurosci 17:1848–1859.

Yeckel MF, Berger TW (1990) Feedforward excitation of the hippocampus by afferents from the entorhinal cortex: redefinition of the role of the trisynaptic pathway. Proc Natl Acad Sci U S A 87:5832–5836.

Zhang YY, Liu MY, Liu Z, Zhao JK, Zhao YG, He L, Li W, Zhang JQ (2019) GPR30-mediated estrogenic regulation of actin polymerization and spatial memory involves SRC-1 and PI3K-mTORC2 in the hippocampus of female mice. CNS Neurosci Ther 00:1–20.

Zhao J, Bian C, Liu M, Zhao Y, Sun T, Xing F, Zhang J (2018) Orchiectomy and letrozole differentially regulate synaptic plasticity and spatial memory in a manner that is mediated by SRC-1 in the hippocampus of male mice. J Steroid Biochem Mol Biol 178:354–368.

Zhou L, Fester L, von Blittersdorff B, Hassu B, Nogens H, Prange-Kiel J, Jarry H, Wegscheider K, Rune GM (2010) Aromatase inhibitors induce spine synapse loss in the hippocampus of ovariectomized mice. Endocrinology 151:1153–1160.

7. Appendix

7.1 List of Abbreviations

°C	Degree celcius
µg	microgram
µL	microliter
µm	micrometer
$µm^3$	cubic micrometer
AB	Antibody
AD	Alzheimer Disease
ANOVA	Analysis of Variance
APS	Ammonium Persulfate
AROM	Aromatase
BPB	Bromophenol Blue
BSA	Bovine Serum Albumin
CA	*Cornu Ammonis*
CNS	Central Nervous System
CO_2	Carbon dioxide
DAPI	4,6-diamidno-2-phenylindole
DG	Dentate Gyrus
DIV	"Days *In Vitro*"
DMP	Delayed Matching to Position
DMSO	Dimethylsulfoxid
DTT	Dithiothreitol
E1	Estrone
E2	Estradiol, 17β-estradiol
E3	Estriol
EC	Entorhinal Cortex
ECL	Enhanced Chemiluminescence
EDTA	Ethylendiaminetraacetat
e.g.	*exempli gratia*
EM	Electron Microscope
ER	Estrogen Receptor
ERα	Estrogen Receptor α
ERβ	Estrogen Receptor β
FBS	Fetal Bovine Serum

GADPH	Glyceraldehyde 3-phosphate Dehydrogenase
GFP	Green Fluorescent Protein
GPCR	*G*-Protein-Coupled Receptor
GPER1	G-Protein-Coupled Estrogen Receptor 1
H_2O	Water
HCl	Hydrochloric acid
HCN	Hyperpolariztion-activated Cyclic Nucleotide-gated
HRP	Horseradish Peroxidase
i.e.	*id est*
IHC	Immunohistochemistry
IgG	Immunglobulin G
ITPKA	inositol-1,4,5-trisphosphate 3-kinase-A
kDa	kilo Dalton
LTP	Long-term Potential
LTD	Long-term Depression
m	minute
M	Mol
mg	milligramm
mL	millilitre
mM	millimolar
Na_2HPO_4	Disodium phosphate
NaH_2PO_4	Monosodium phosphate
$NaHCO_3$	Sodium bicarbonate
NaOH	Sodium hydroxide
NC	Nitrocellulose
NGS	Normal Goat Serum
nm	nanometer
nM	nanomol
NP40	Nonyl Phenoxypolyethoxylethanol
OsO_4	Osmiumtetroxide
P	Postnatal
PB	Phosphate Buffered
PBS	Phosphate Buffered saline
PBS-T	Phosphate Buffered Saline-Tween
PFA	Paraformaldehyd
pH	potential of hydrogen
PP	Perforant Path

PS	Penicillin-Streptomycin
PSD95	Postsynaptic Density 95
rcf	relative centrifugal force
resp.	respectively
RIPA	Radioimmunoprecipitation Assay
RT	Room Temperature
s	second
SC	Schaffer Collaterals
SDS	Sodium Dodecylsulfate
SDS-PAGE	Sodium Dodecyl Sulfate Polyacrylamide Gel Electrophoresis
SEM	Standard Error of Mean
SL	Stratum ucidum
SLM	Stratum lacunocum-moleculare
SNAP25	Synaptosomal nerve-associated protein 25
SO	Stratum oriens
SP	Stratum pyramidal
SR	Stratum radiatum
TA	Temporoammonic path
TEMED	Tetramethylethyldiamin
Tris	Trishydroxymethyl-aminomethan
V	Volt
WT	Wild type

7.2 Index of Figures and Tables

7.2.1 Figures

7.2.2 Tables

8. Acknowledgement

I would like to express my sincere thanks to all those people who supported me to complete this work.

Many thanks to Prof. Dr. Gabriele Rune for giving me the opportunity to do my doctoral thesis at the Institute for Neuroanatomy and the important suggestions during the project.

I would like to give my sincere gratitude to Prof. Dr. Roland Bender. Thank you for the professional guidance and kind support, for the valuable and timely suggestions, for the remarkable patience and encouragement.

Many thanks to my colleagues at the Institute for Neuroanatomy. A special thank you to Dr. Lepu Zhou: Thank you for your tireless help and also the important advice for life. Of course, I also want to express my sincere gratitude to the technician assistances. Thanks a lot for the experimental guidance, so that I have grown up from a beginner who know nothing about experiment to a "scientist" who can solve various problems.

I would like to express my grateful thanks to my former supervisor Prof. Baoan Chen and all the Chinese Friends during my stay in Germany. Thank you very much for the support and encouragement. Because of you, I have never felt alone in a foreign country.

I would like to thank the Chinese Scholarship Council (CSC) for the financial support, so that I can study without any worries and anxieties related to money.

Last but not least, I would like to give my deepest gratitude to my family. Thank you for always respecting my decisions, trusting me unconditionally, supporting me and encouraging me. Because of your unwavering love and firm support. I always have endless strength and courage when facing difficulties.

9. Curriculum Vitae

Lebenslauf entfällt aus datenschutzrechtlichen Gründen.

10. Eidesstattliche Versicherung

Ich versichere ausdrücklich, dass ich die Arbeit selbständig und ohne fremde Hilfe verfasst, andere als die von mir angegebenen Quellen und Hilfsmittel nicht benutzt und die aus den benutzten Werken wörtlich oder inhaltlich entnommenen Stellen einzeln nach Ausgabe (Auflage und Jahr des Erscheinens), Band und Seite des benutzten Werkes kenntlich gemacht habe.
Ferner versichere ich, dass ich die Dissertation bisher nicht einem Fachvertreter an einer anderen Hochschule zur Überprüfung vorgelegt oder mich anderweitig um Zulassung zur Promotion beworben habe.
Ich erkläre mich einverstanden, dass meine Dissertation vom Dekanat der Medizinischen Fakultät mit einer gängigen Software zur Erkennung von Plagiaten überprüft werden kann.

Unterschrift: ....